KfK 4876
Juni 1991

Investigations of Structural Flow Instability at High Temperatures

M. Bocek, J.-H. Choi
Institut für Material- und Festkörperforschung

Kernforschungszentrum Karlsruhe

KERNFORSCHUNGSZENTRUM KARLSRUHE

Institut für Material- und Festkörperforschung

KfK 4876

Investigations of Structural Flow Instability at High Temperatures

Michael Boček, Jae-Ho Choi

Kernforschungszentrum Karlsruhe GmbH, Karlsruhe

Kernforschungszentrum Karlsruhe GmbH
Postfach 3640, 7500 Karlsruhe 1

ISSN 0303-4003

Abstract.

The stability of high temperature plastic flow is examined by means of a dislocation population model.The energy ratio $\lambda \equiv W/W_s$ (expended to stored energy) which is considered as a measure for the distance from thermodynamical equilibrium appears as the characteristic quantity of the model.From the view of the model,instability of deformation structure (structural instability)–which gives rise to macroscopic flow instability–is the consequency of the exhaustion of energy storage capability. Structural instability appears to be a critical phenomenon initiated by the growth of (critical) fluctuations in size d_s of deformation substructure.This is suggested to occur at a critical value λ_m^* which should be independent of the loading procedure. The critical value depends of stress and structural parameters respectively and is in the range from 20 to 100.In accordance with model expectations the observed critical λ^*–values for different materials are within the margins of λ_m^* and,in accordance with the model, these are proportional to the critical stress σ^* and are independent of loading procedure and loading path respectively.Hence λ^* reveals properties of a quantity of state.*In situ* examinations conducted on polycrystalline copper at $T_h > 0.4$ have shown that the strain distribution during flow instability is macroscopically uniform.This indicates a high growth rate of critical fluctuations at higher temperatures.There is indication that the size d_s^* of the dislocation substructure at criticality is proportional to the grain size d_g.Although this behaviour is not being understood at present,it seems to be supported by direct evidence.

Untersuchungen zur strukturellen

Fließinstabilität bei hohen Temperaturen.

Mittels eines Versetzungs–Populationsmodells wird die Stabilität der Hochtemperaturverformung untersucht. Der charakteristische Systemparameter $\lambda=W/W_s$ ist das Verhältnis der Verformungsenergie zur gespeicherten Energie. Dieses kann als ein Maß betrachtet werden für den Abstand des System vom thermodynamischen Gleichgewicht. Dem Modell zufolge ist strukturelle Instabilität – die sich makroskopisch als Fließinstabilität äußert – bedingt durch die Erschöpfung der Energiespeicherfähigkeit. Erstere ist ein kritisches Phänomen, bewirkt durch das Wachstum kritischer Fluktuationen der Verformungssubstruktur. Ein solches erfolgt für kritische Werte des Parameters λ_m^*, die von der Versuchsführung unabhängig sein sollten. Dem Modell zufolge ist λ_m^* spannungsabhängig, mit Werten im Bereich zwischen 20 und 100. In Übereinstimmung mit dem Modell sind die experimentellen λ^*–Werte unabhängig von der Verformungsweise und vom Verformungsweg; sie liegen für verschiedene Materialien in dem vorhergesagten Bereich der λ_m^*–Werte, und sie sind proportional zur kritischen Spannung σ^*. Somit besitzt λ^* Eigenschaften einer Zustandsgröße. *In situ* Untersuchungen an Kupfer bei $T_h>0.4$ bestätigten, daß die Dehnungsverteilung während der Fließinstabilität makroskopisch gleichförmig ist. Daraus ist auf eine große Wachstumsrate kritischer Fluktuationen zu schließen. Möglicherweise ist die kritische Größe der Substruktur proportional zur Ausgangskorngröße des Materials.

Investigations of Structural Flow Instability at High Temperatures.

Michael Boček and Jae–Ho Choi

Kernforschungszentrum Karlsruhe,
Institut für Material– und Festkörperforschung
Postfach 3640,D–7500 Karlsruhe 1,FRG

1.Introduction

1.1 Model description

Because associated with defect production,plastic flow *reduces* the lattice order on an *atomic scale.*In contrast,however,a *large scale defect ordening* takes place during deformation revealing as dislocation *patterning* (see e.g.[1]).Novel dynamical approaches consider deforming materials as open,non linear systems with many degrees of freedom driven *far from thermodynamical equilibrium.*In this case stationarity of the non equilibrium state is *not* produced by *energy minimization* [2] but by the *interplay of system elements* which gives rise to a large scale *self organized defect order* (patterning) [3–6].Rather than to examine the mechanism of patterning the investigation deals with the problem of *dynamical instability* of deformation patterns.

As a matter of fact,materials submitted to stationary (external) loading conditions may respond non monotoneously,i.e.their plastic flow behaviour alternates between periods of work hardening and softening respectively.This is associated with destabilization and reproduction of stable deformation structures, paradigmatically revealed in dynamic recrystallization (DRX).Accordingly,the plastic regime switches between stability and instability resp.,obviously revealing the feature being typical for *bifurcation phenomena.*In order to explain this very general observation one of the authors [7]

proposed a model which presumes a stationary dislocation substructure which is characteristic for a the steady state plastic regime.*Mobile* dislocations are considered as the *relevant* defect population.The *generation* and annihilation of dislocations is suggested to take place preferentially in *dislocation walls.*Thus we may suggest that $\rho \propto \rho_w$, where ρ_w is the density of wall dislocations.The corresponding rate equation is

$$\dot{\rho} = \dot{\rho}^+ + \dot{\rho}^-$$

where $\dot{\rho}^+ \propto \rho$ and $\dot{\rho}^- \propto \rho^2$ is the production– and annihilation rate of mobile dislocations resp.These are equal in the stationary regime.In reality both the mechanism are discontinuous in time and hence the temporal evolution of mobile density is more appropriately described by the non linear *difference* equation (logistic equation)

$$N_{t+1} = \alpha N_t(1-N_t)$$

t numbers the generation and $N_t = \rho_t b/a = \rho_t/\rho_{ss}$ is the normalized dislocation density.a,b are the rate constants of dislocation production – and annihilation respectively. $\rho_{ss} = a/b$ is the steady state density which would be achieved in stable flow (see ref.7). α is the system parameter containing the (external) loading conditions as well as structure parameters.The system operates in the way that mobile dislocations from the preceding production step (t) are being the seed for the next one (t+1) and so forth. This iterative procedure is carried out repeatedly untill a *stationary equilibrium density* N_e will establish (i.e. $N_{t+1}=N_t=N_e= \rho_e/\rho_{ss}$).The value of N_e is completely determined by the system parameter α.

As shown in Fig.1 below the critical α^*–value (=3) $N_e(\alpha)$ is a single– and above α^* a multi–valued function of α.Correspondingly, depending of loading conditions and deformation structure, $N_e(\alpha)$ reveals *bifurcations.*Because associated with a change in ρ_e,the bifurcation gives rise to structural instability,which macroscopically may reveal

as flow *instability*.Hence the model correlates criticality ($\alpha=\alpha^*$) with structural instability.

The bifurcation diagram shown in Fig.1 consists of three branches.The first one for "subcritical" α–values ($1 \leq \alpha < 3$) is characteristic for structural stability.In this branch the linear term in the rate equation,i.e. the production rate dominates.Local non–equilibria between production and annihilation rate of dislocations – which will give rise to fluctuations in the size d_s of the deformation substructure–are smoothed out by local compensation leaving the whole in dynamical equilibrium.[1]

The bifurcation region ($3 \leq \alpha \leq 4$) shows two branches .The upper one with the highest possible equilibrium density $\rho_{e,max}$ and the lower with the lowest possible density $\rho_{e,min}$.Between these two branches cascades of bifurcations appear (for details the reader is refered to ref.7). Hence with a particular critical α–value at least two equilibrium densities are correlated.In the bifurcation region the non–linear term (annihilation) dominates the rate equation.In contrast to the preceding case, deviations from local equilibrium,i.e $\delta\dot{\rho}$,will amplify.It is an inherent property of non–linear, dissipative dynamical systems that with *increasing distance from thermodynamical equilibrium* for critical α–values growth rate perturbations (in this case $\delta\dot{\rho}$) become *unstable*.In contrary to subcriticality, fluctuations in cell size d_s are *not asymptotically stable*.They increase with time and spread through the material giving rise to a non–equilibrium "phase transition".

As shown in ref.7 the system parameter α for high temperature flow is expressed by

---

[1]Regimes close to thermodynamical equilibrium ,characterized by small α–values,share the important property of *asymptotic stability*.In this range the system is capable of damping internal fluctuations by means of *detailed equilibria* [18].For this reason this branch of states is sometimes called the *thermodynamic branch*.

$$\alpha = (2/Gb^2 pZ\rho_w)W \tag{1}$$

where G is the shear modulus,b is the Burgers vector and W is the expended deformation energy and

$$p(\sigma) = L/d_s \tag{2}$$

L is the mean dislocation path and d_s is the linear dimension of the deformation substructure and Z = 23 [8] is an empirical constant in the relationship

$$d_s/b = Z(G/\sigma) \tag{3}$$

The ratio of *expended* energy W to *stored* energy W_s

$$\lambda \equiv W/W_s \tag{4}$$

by the 1.Law of thermodynamics is connected with the energy Q_d dissipated as heat in the way

$$-Q_d = W(1 - 1/\lambda) > 0$$

where for $Q_d = 0$ (*elastic* case) $\lambda = 1$ and for $-Q_d/W = 1$ (*plastic* case) λ is unbounded.Therefore λ can be considered as a measure for the *distance from thermodynamical equilibrium* (TDE)[9].

Inserting into eq(4) for W_s the energy stored in *dislocation walls* [30]

$$W_s = (Gb^2/4\pi)f(\nu)\ln(L_w/b)\rho_w \tag{5}$$

the combination of the above equations (with $f(\nu)$=1.2 and L_w/b=50) gives the *model* value

$$\lambda_m = 1.44\ \alpha pZ \tag{6}$$

Because depending of λ the parameter α is in principle accessible to measurements. In a regular cell structure formed by a stuck of cubic cells of the edge length d_s,wall density ρ_w and mean distance L_w of wall dislocations obey the relationship

$$\rho_w = 4/d_s L_w \tag{7}$$

If in eq(2) $L = L_o$ is considered constant,explicitely independent of σ,one obtains from

the above

$$\lambda_m = \alpha L_o Z/0.7 d_s = 1.4\alpha(L_o/Gb)\sigma \qquad (8)$$

At criticality i.e.for $\alpha=\alpha^*=3$,it is

$$\lambda_m^* = 4.2\,(L_o^*/Gb)\sigma^* \qquad (9)$$

The proportionality betweem $\lambda_m^*$and σ^* can be checked by experiments and hence,in view of the model assessment,eq (9) plays an important role.From eq(6) a gross estimate with p = 0.5 gives a critical model value

$$\lambda_m^* = 50$$

However due to the stress dependence of p λ_m^* may be within the range between 20 to 100.According to eq(9) the experimental λ^*–values should be proportional to σ^* and independ of loading procedure.λ^*,if at all,should be temperature dependent essentially through $\sigma^*(T)$ and according to the model $d\lambda^*/d\sigma^*$ is expected to depend of the structural quantity L_o^*.

1.2 The energy ratio λ

In contrast to what is required in view of the present task,most of the stored energy data W_s stem from materials deformed at *low* homologous temperatures $T_h = T/T_m$. However from measurements of Williams [10] some data about the dependence of W_s upon the expended energy W and the temperature T can be obtained in the temperature range $0.14 \leq T_h \leq 0.50$.Williams,using metals with different melting temperatures T_m,determined at room temperature T the increase of W_s associated with different amounts of deformation energy W(1) and W(2) respectively.Therefrom, as shown in Fig.1 of ref.9,a linear relationship between W_s and $(1/T_h)^2$ is derived. Furthermore,in agreement with experimental observations on polycrystalline materials where $W_s \propto W^{1/2}$[11],the ratios $W_s(1)/W_s(2)$ turned out to be approximately equal to $(W(1)/W(2))^{1/2}$.Then from Fig.1 in ref.9 it follows

$$W_s / W^{1/2} = a_o T_h^{-2} = a_T / T^2 \equiv a_m \tag{10}$$

where $a_o = 5.8\text{x}10^{-2}(\text{J/gatom})^{1/2}$ and $a_T = a_o T_m^2$. One obtains

$$\lambda \equiv W/W_s = W^{1/2}/a_m = W_s/a_m^2 \tag{11a}$$

and for the critical value

$$\lambda^* = (W^*)^{1/2}/a_m = W_s^*/a_m^2 \tag{11b}$$

where W_s^* is the *energy storage capacity* and

$$W^* = \int_0^{\epsilon^*} \sigma(\epsilon) d\epsilon \tag{12a}$$

is the mechanical work expended (per unit volume) to instability. The *relative* difference between W_s^* and W_s can be considered as the *energy storage capabilty*

$$\chi_s = (1 - \lambda/\lambda^*) \tag{12b}$$

which in the course of deformation linearly decreases with λ.

Defining the *energy storage rate* by

$$\Gamma_s \equiv dW_s/dW = 1/2\lambda \tag{12c}$$

Γ_s decreases from an initially high value $\leq 1/2$ to a low critical value

$$\Gamma_s^* = 1/2\lambda^* = a_m^2/(2W_s^*) \tag{12d}$$

for which $(\lambda = \lambda^*)$ the energy storage capability χ_s is exhausted. Hence the structural *stability criterion* can be suggested [9]

$$W_s < W_s^* \quad \text{or} \quad \Gamma_s > \Gamma_s^* \qquad \text{stable} \tag{12e}$$

Combining eqs(5) and (12b) and taking into account that $\rho_w = \rho_w(\sigma(\epsilon))$ one obtains

$$\Gamma_s^* = 1/(2\lambda^*) \propto F(\sigma)\, h^*/\sigma^* > 0 \tag{12f}$$

where $h^* = (d\sigma/d\epsilon)_{\sigma^*}$ and $F(\sigma) > 0$ depends of $\rho_w(\sigma)$. Obviously because λ^* is finite it is $h^* > 0$. Therefore structural instability does not occur at the peak stress σ^*. In agreement with microstructural examinations [15][27][29] it follows from linear stability analysis that growth of critical fluctuations in substructure starts at a stress σ_c which is closely

below σ^* (see chapter 2.5).Hence the present experimantal λ^*–values are somewhat overestimated.

2.1 Testing procedures

Following procedures were applied: tensile strain controlled (STC) tests; load controlled (LDC) tests; change in loading conditions (CLC) experiments and strain controlled low cycle fatigue (LCF) experiments .

2.2 Material and test conditions

The experiments were conducted on following materials:

a)Cu polycrystals (PC);mean grain size, $d_g=1,6.10^{-5}$m; main impurities were 0,015 C;0,021 O;<0,001 N;

b)Cu single crystals (SC) (same purity as PCs,random orientation);

c)Ni–PC;$d_g=2,1.10^{-4}$m; (0,014 C;0,008 O;<0,005 N);

d)Cd–PC,$d_g=1.5x10^{-4}$m;

e)Pb–PC,$d_g=9.7x10^{-4}$m (inhomogeneous grain structure);

f)solution annealed austenitic steels type DIN 1.4909; $d_g=1,2.10^{-4}$m and DIN 1.4981; $d_g=2x10^{-5}$m.

The own experiments cover:

the temperature range $0.17 \leq T_h \leq 0.87$;

the strain rate range: $1.3x10^{-5} \leq \dot{\epsilon} \leq 3.7x10^{-1}$(1/s) ;

the stress range: $2.7x10^{-4} \leq \sigma^*/G \leq 8.3x10^{-3}$.

The test on Cu and Ni were conducted in a vacuum furnace at a pressure of $1.3x10^{-3}$

Pa. For comparison Cu–PCs were also deformed in air atmosphere up to 500^{o}C.Steels,Cd– and Pb specimens were deformed in air.In addition data from literature were evaluated from: Cu–SC;STC test [12,13,14,15];Ni–SC;STC tests [13]; Ni–PC; torsion [16]; Al–PC;torsion [17] and LDC tests [25].These were included in Table 1.The paper presents results of investigations of the influence loading conditions have upon the experimental λ^{*}–values.

2.3 Experimental results

2.3.1 Validity of the empirical $W_s(W)$ relationship

The evaluation of the experimental λ–values is based on the empirical relationship eq(10).The validity of eq(10) will be checked by means of the ratio ϵ^*/σ^*. The latter can be *calculated from the model* and compared with (model independent) *experimental values* taken from the $\sigma(\epsilon)$ diagram (see e.g.Fig.2.)

According to eq(11b) and (12a) it is for the STC test

$$\lambda^{*}=(V_m\int_0^{\epsilon^*}\sigma(\epsilon)d\epsilon\,)^{1/2}/a_m.$$

As shown in ref.9 for the present test conditions the experimental $\sigma(\epsilon)$ curves can be properly expressed by $\sigma = \sigma_0 + \eta\epsilon^{1/2}$,and for $2(\sigma^*/\sigma_0)>>1$ it is approximatelly $\int_0^{\epsilon^*}\sigma(\epsilon)d\epsilon \cong (2/3)\sigma^*\epsilon^*$,where σ_0 is the initial flow stress.Hence $\lambda^{*} \cong (2/3\ V_m\sigma^*\epsilon^*)^{1/2}/a_m$ and therefrom we derive

$$d\epsilon^*/d\sigma^* + \epsilon^*/\sigma^* - K(\epsilon^*/\sigma^*)^{1/2} = 0 \qquad (13)$$

with

$$K = (d\lambda^{*}/d\sigma^*)0.14/(V_m^{1/2}\,T_h^2) \qquad (14)$$

where V_m is the gramatomic volume.The solution of eq(13) for K = constant $\neq f(\sigma^*)$ (i.e. for $\lambda^{*} \propto \sigma^*$ (see eq(9)) gives

$$\epsilon^*/\sigma^* \equiv k_{\epsilon^*} = (K/2)^2 \qquad (15)$$

what,as shown in Fig.3,in deed is independent of σ^*.In Table 1 the k_{ϵ^*}–values calculated from eq(14) can be compared with the experimental values (see also Fig.4).Although these cover a range of 4 orders of magnitude,for all the materials examined the agreement is excellent and hence,for the present test conditions,the validity of the empirical relationship (10) is considered to be confirmed.

2.3.2 STC and LDC experiments

STC–tests

In Fig.5a several stress/strain curves revealing flow instabilities are shown for a variety of materials.For given grain size the number and shape of the stress peaks in STC tests depends of loading conditions.As a matter of fact,for given loading conditions there is preference for fine grained material to exhibit multi–peak (MP) instabilities,whereas coarse grained specimens rather reveal single–peak (SP) behaviour.Moreover the flow behaviour SP/MP obviously depends also upon the size of the specimen.As shown by Choi [28] on Ni PCs a large ratio of grain size to the cross section of the specimen favours MP behaviour.Observations by video–technique (see chapter 2.6.2) have shown that for temperatures $T_h \geq 0.4$ the stress peaks were not associated with necking which definitely marks failure (see Fig.11b).As can be realized from Fig.4 and Fig.5b the range of the λ^*–values associated with the first σ–peak is for different materials within that predicted by the model.One should mention that Al deformed by *torsion* fits into this picture as well.For Cu–PCs the reproducibility of the λ^*_{STC}–values have shown to be as good as that e.g. for the yield strength.The standard deviation $\Delta\lambda^*$ for λ^*_{STC} at 500^oC is ± 4%.

As shown in Fig.4 in accordance with the model (see eq(9)) in the STC test the

experimental λ^*–values are proportional to σ^* and in LDC tests these are proportional to the nominal creep stress σ_0.The slopes $d\epsilon^*/d\sigma^*$ are dependent of temperature. This,from the view of the model,should be attributed to the temperature dependence of K (see eq (15)).The latter,according to eq (14) is proportional to $d\lambda^*/d\sigma^*$ and to T_h^{-2}.K possibly depends of T indirectly through $d\lambda^*/d\sigma^*$.Because $d\lambda_m^*/d\sigma^*$ is proportional to L_o^* (eq(9)) we may suggest that the temperature dependence of $d\lambda^*/d\sigma^*$ is to some extend due to $L_o^*(T)$ however the main influence is supposed to be due to $\sigma^*(T)$.As shown in Fig.6 for the materials examined σ^* for $T_h \geq 0.4$ is proportional to $1/T_h^2$.Putting $d\lambda^*/d\sigma^* = d\lambda_m^*/d\sigma^*$,in Table 1 the L_o^*/b–values are listed which were calculated by means of eq(9).These reveal the temperature dependence of $d\lambda^*/d\sigma^*$ and,for comparable loading conditions,they depend of the material.

For the materials examined the range of the grain size d_g extends over two orders of magnitudes (see Table 1).In order to investigate an influence of d_g upon $d\lambda^*/d\sigma^*$ the ratio (see eq(2))

$$(L_o^*/d_g)/p = Gb(d\lambda^*/d\sigma^*)/(p\, d_g 4.2) = (d_s^*/d_g)$$

is listed in Table 1.As one can realize the influence grain size has upon L_o^* is eliminated in the gross.Moreover,from the above one copuld suggest,that d_s^* is correlated with d_g.To eliminate the influence of temperature upon L_o^* due to $\sigma^*(T_h)$– which is shown in Fig.6– the d_s^*/d_g– values calculated with p=1 (see above) are multiplied by $1/T_h^2$ and these,in Fig.7,are plotted vers.T_h.Within the range of temperatures examined i.e. $0.17 \leq T_h \leq 0.99$ they obviously are independent of temperature and accordingly $L_o^*/d_g \propto d_s^*/d_g \propto T_h^2$.

Two groups of materials appear.For fine grained specimens the calculated $(d_s^*/d_g)/T_h^2$–values are approximately 5 times that for the coarse grained specimens.In Fig.7 *experimental* $(d_s^*/d_g)/T_h^2$–values for fine grained Ni [26] and coarse grained Al [25] are

shown as well.They fit into the corresponding groups of calculated values.From the comparison of the experimental and calculated values for Al the p–value from the above equation can be estimated.It is for p=1

$$(d_s^*/d_g)_{cal}=Gb(d\lambda^*/d\sigma^*)(4.2\ d_g)=0.011$$

for the experimental value we have

$$(d_s^*/d_g)_{exp}=(1/p)\ (d_s^*/d_g)_{cal}=0.060$$

and therefrom p≃0.2.From the view of the model this indicates that whereas in fine grained materials the mean free path $L_o^* \simeq d_s^*$,probably in coarse grained material k<1;e.g. for Al PC in Table 1 it is $L_o^* \simeq d_s^*/5$.Accordingly for coarse grained Cd and Ni one would expect that (d_s^*/d_g)–values calulated with p=0.2 would be within the range of the corresponding values for the fine grained material what actually is the case as shown in Fig.7.

Recently Sakai and Ohashi [26] by TEM observations have shown that the size d_s^* of the deformation substructure of Ni–PCs is closely related to the size d_R of the grain structure *resulting from structural instability* (dynamic recrystallization).Hence according to own investigations – which indicate that d_s^* is related to d_g – it seems that d_R could be correlated with d_g.

At low temperatures the comparison of measured and calculated values like $d\lambda^*/d\sigma^*$,$d\epsilon^*/d\sigma^*$ and $(d_s^*/d_g)T_h^{-2}$ shows that certain "high temperature" model predictions are valid also for temperatures T_h<0.4 (see Table 1).This obviously is less surprising and indicates that exhaustion of energy storage capability is rather a general phenomenon of crystal plasticity,largerly independent upon the details of particular micromechanisms.

LDC–tests

Flow instabilities in LDC tests are associated with a fast increase of strain rate (Fig.8).As suggested by Boček and Choi [20] structural instability leads to a change of the effective stress σ_e.This in the STC test increases during the stress drop and in case of MP instability σ_e decreases as deformation proceedes from the stress minimum to the next stress peak.Because the strain rate $\dot{\epsilon}$ is governed by σ_e in the LDC test (for MP behaviour) $\dot{\epsilon}$ reveals a maximum (Fig.8).For SP instability σ_e does not decrease after the load drop and accordingly in the LDC test $\dot{\epsilon}$ will not reveal a maximum.In contrary, due to the sensitive stress dependence of the strain rate,thelatter proceedes to increase (sometimes however a scarce dwell period for $\dot{\epsilon}$ may appear) and hence the flow instability coincides with the accelerated creep range.This is the reason for why flow instability in LDC tests usually escapes observation.In Fig.4 λ^*_{LDC}–values are plotted versus the nominal creep stress σ_0 and the λ^*_{STC}–values vers.σ^*.The former fit the $\lambda^*(\sigma^*)$ dependences from the STC tests.As can be realized from Table 1,λ^*–values from torsion tests on Al agree with the predicted stress dependence.This is in strong support of the model expectation that criticality is a phenomenon which is independent of *loading procedure.*

2.3.3 LCF experiments

In order to investgate whether λ^* does depend upon the *strain path* strain controlled LCF tests were conducted in addition.In Fig.9 for Ni–PCs loaded with different total strain amplitudes $\Delta\epsilon_t$ the corresponding cyclic hardening curves are shown .The upper scale correlates the stress amplitudes σ_{max} with the number of cycles N and the lower one correlates σ_{max} with λ_{LCF}. The critical values were calculated from

$$\lambda^*_{LCF} = a_m^{-1}(W^*_{LCF})^{1/2}$$

For the present case the deformation energy $W_c \approx W^*_{LCF}/N^*$ expended per cycle is practically independent of N.However W_c depends of $\Delta\epsilon_t$ and because W^*_{LCF} is fairly

constant independent of $\Delta\epsilon_t$,the flow instabilities in Fig.9 (with the respective λ^*_{LCF} –values 38 and 48) appear at different N^*–values.

In Table 2 the results of several LCF experiments conducted on Ni–PCs at 750°C are summarized.As expected,the number of cycles to instability N^* increases with decreasing W_c.The λ^*_{LCF}–values fit into the range of λ^*_m–value moreover,as follows from Table 1,the $(\epsilon^*/\sigma^*)_{LCF}$– and $(\lambda^*/\sigma^*)_{LCF}$–data from LCF tests listed in Table 2 compare very well to those from STC tests.This and the agreement between results from *torsion*–and *unidirectional* tests obviously confirms the *independency of* λ^* *upon strain path*[2].

2.3.4 Experiments with change in loading conditions (CLC–tests)

In order to investigate whether there is an influence of the *loading path* upon λ^*,experiments were performed with change in loading procedure.For illustration, in Fig.10 the result of a CLC test is shown in which,at a constant temperature of 500°C, the loading procedure was changed from LDC– to STC type.The latter can be compared with the STC reference test.In the first loading step the Cu–PC was crept at $\sigma_0=0.89\sigma^*$ to instability ($\lambda^* \approx 35$ and σ^* refer to the STC reference test resp.) and thereafter loading proceeded in the STC mode.The comparison with the reference STC test shows that the flow instability at the interruption of the LDC test correlates with

---

[2]In addition to *thermodynamical irreversibility* manifesting in energy dissipation,strain cycling is associated with *kinematic irreversibility* of dislocation motion.According to the above it doesnot seem that the latter plays any significant role in the phenomenon considered.Rather than the mechanism of substructure formation it is the capability of substructure for energy storage which is relevant for structural stability.

that in the STC experiment.

In Table 3 results of CLC experiments performed on Cu–PCs at $T_o = 400^oC$ are shown.In the upper two lines the reference values λ_R^* for the respective loading procedures are listed.$W_o < W^*$ is the (independent) deformation energy of the initial loading step. W_1 is the deformation energy of the consecutive loading step necessary to produce flow instability.The resulting λ_{CLC}^* –values were calculated from

$$\lambda_{CLC}^* = (W_o/a_{m,o}^2 + W_1/a_{m,o}^2)^{1/2} = a_{m,o}^{-1}(W_o + W_1)^{1/2} \qquad (16)$$

These,as one can realize from Table 3,are independent of the sequence of loading steps.The results show that changes in loading procedure carried out at constant temperature do not influence the λ^*–value.In conclusion:λ^* turns out to be independent of loading procedure,loading path and strain path respectively.Hence λ^* reveals the property of a quantity of state.

2.4 Single crystals

As shown in Fig.11a flow instability does occur also in single crystals.The shape of the corresponding $\sigma(\epsilon)$–curves reveal sharp stress dips following a stress peak.The same behaviour is observed on PCs at very high temperatures (Fig.11b).This obviously is associated with grain coarsening [20].There is evidence from TEM investgations on Cu–SC [21] that networks of well developed dislocation walls are prerequisite for flow instability to occur.As recently confirmed on Cu [15] for comparable conditions the strain to generate such networks is much less in PCs.This obviously is in support of the observation shown in Fig.11a that for same loading conditions the strain to criticality ϵ^* –in accordance with observations by other authors [15][19]– appeares to be substantially less for PCs.However once an instability has been produced the follow–on istability needs much less strain than for the first one,what underlines the importance

of substructure for energy storage.Data for Cu SCs of random orientation are collected in Table 4.The experimental λ^* values are within the range of the model value λ^*_m.

2.5 Flow instabilities

It is the connection between deformation structure and flow behaviour which makes structural changes "macroscopically" observable.The basic step toward the *mechanistic* understanding of flow instabilities is the analysis of the *local* constitutive equation

$$d\sigma = Hd\epsilon + \Psi d\log\dot{\epsilon} \tag{17}$$

where

$$H = (\partial\sigma/\partial\epsilon)_{\dot{\epsilon},\phi,T} \tag{18a}$$

$$\Psi = (\partial\sigma/\partial\log\dot{\epsilon})_{\epsilon,\phi,T} \tag{18b}$$

This correlates the *external* variables: flow stress σ,total strain ϵ and strain rate $\dot{\epsilon}$.The index ϕ indicates that the change does occur at constant deformation structure.The quantities H and Ψ are *per definitionem* dependent of coordinates and these,in general,are not equal to the corresponding experimental quantities h and ψ.

For the STC test (in the z–direction) the description is completed by the "machine equation"

$$\dot{\sigma}(t)/M + (1/l)\int_0^l \dot{\epsilon}_p(z,t)dz \equiv I \tag{19}$$

M is the combined modulus;,l is the gauge length for t>0.Because responding to the load which is independent of z,local inhomogeneities in material properties– which take an influence upon the local flow stress $\sigma(z,t)$– are not "recognized" by the machine.With other words,the device does not discern between the "geometric length" l(t) and the "active length" $l_a(t)$ of the specimen.If the plastic strain rate $\dot{\epsilon}_p$ is independent of z (uniform strain) it is $I = v_m/l_o \equiv \dot{\epsilon}_o$,where v_m is the cross head velocity

of the machine amd l_o is the gauge length at t=0.For $l_a < l$ the strain is localized (shape instability).Because in this case the total local strain rate $I(z,t) \equiv \dot{\epsilon}(z,t) = v_m/l_a > \dot{\epsilon}_o$ the load must drop (strain rate instability).Usually strain rate instability is attributed to strain localization. However,as shown in this examination, in general strain rate instability can occur at *macroscopically* uniform strain.For a review on this subject the reader is refered to ref.22 and 23 respectively.

For small perturbations $\delta\epsilon$ from uniform strain which may originate from fluctuations in substructure,linear stability analysis leads to [23]

$$\delta e = \delta\epsilon_o \exp(\gamma t)$$

where the Liapunov exponent

$$\gamma = \delta\dot{\epsilon}/\delta\epsilon = [(\sigma - H)/\Psi]\dot{\epsilon} \qquad (20a)$$

is decisive for the onset of instability,i.e. for the growth of citical perturbations.Accordingly the criteria are derived from the above

$$\begin{array}{l} >0 \text{ unstable} \\ \gamma = 0 \text{ critical} \\ <0 \text{ stable} \end{array} \qquad (20b)$$

Assuming parabolic work hardening

$$\sigma = \sigma(o) + \eta\sqrt{\epsilon} \qquad (21)$$

where η is a temperature dependent parameter,then from eq(8) for γ=0 the critical strain to nucleate a neck is

$$\epsilon_N = (1/2)\left\{(\sigma(o)/\eta)^2\left[1 - \left[1 + 2(\eta/\sigma(o))^2\right]^{1/2}\right] + 1\right\} \qquad (22)$$

In Fig.12 for a Cu –PC deformed at 500°C the $\sigma(\epsilon)$ curve is shown together with the strain dependency of the corresponding work hardening coefficient $h \equiv d\sigma/d\epsilon$.According to the above,strain localization is expected to occur within the hatched strain intervals.As follows from Fig.12 criticality i.e. $\sigma_c = h_c$ (with regard to eq(12f) note that $\sigma_c = h_c < \sigma^*$) is already achieved at a strain $\epsilon^* = 0.12$. Necking, however,is observed at a strain $\epsilon_N = 0.39$ which agrees well with the strain for nucleation of necking,calculated

from eq(22) (with $\sigma(o)$=20MPa and η=160MPa).However inserting ϵ_N=0.39 into eq(21) one obtains σ_N=120 MPa what is to be compared with the stress at criticality $\sigma_c \leq \sigma^*$=55MPa.Hence the flow instability at ϵ^*=0.12 can not be *predicted* from the above consideration. According to the present model,due to exhaustion of energy storage capability ,the flow stress σ doesnot approach σ_N=120MPa.Structural instability will keep σ below this value.Hence,as shown in Fig.12,the experimental stress/strain curve severly deviates from that given by eq(21).

However the criterion for criticality (20b) can be used to determine the correct critical stress value σ_c.For practical reasons,throughout this investigation σ^*– and ϵ^*–values were used to evaluate λ^*–values which consequently are slightly overestimated.The critical distance determined by means of eq(12a) using the ϵ_c–value from Fig.12 is λ_c=32 (the index c indicates that the critical λ–value is determined by means of (20b)),which is 3% less than λ^*.hence the differnce is within the standard deviation for λ^*_{STC}–values (see chapter 2.3.2).In general the difference will depend of the shape of $\sigma(\epsilon)$ close to instability.

2.6 Strain distribution

2.6.1 Testing procedure

A video record was used to examine the shape change of the specimen in the course of deformation.The optical system seized 1/3 of the specimens length (middle section).The evaluation of the diameter was carried out on the screen with a precision of ±1mm what corresponds to a resolution of diameter change of $\Delta(2R) \approx \pm 4 \times 10^{-2}$mm. The corresponding radial strain resolution was $\Delta\epsilon_R = \pm\, \Delta(2R)/(2R_o) \approx \pm 4 \times 10^{-3}$.For technical reasons the examination was performed in air atmosphere at temperatures 300°C,320°C and 340°C at a strain rate $\dot{\epsilon}_o = 3.3 \times 10^{-4}$/s.Under these conditions and

for test durations t_{ox} of 20 to 30 minutes,growing oxide layers escaped observation.An estimate of the thickness d_{ox} of the layer means of data from ref.24 for 340°C and and for $t_{ox}=1.8x10^3$s gives $d_{ox}\approx 3x10^{-3}$mm,what is 10 times less than the resolution power of the present method.

2.6.2 Results

The measurements were performed in 6 equidistant (1.5mm) positions adjusted in the middle section (approximately 8mm long) of the specimen,were–by experience–strain localization was expected to occur.Denoting by $\Delta t=t_i-t_{i+1}$ the time interval between to successive measurements,then

$$\{\dot{R}\} \equiv 2(R_1-R_2)/\Delta t$$

is the average change of the diameter in Δt.In Fig.13,for the differnt positions,the diameter 2R of the specimen is plotted versus t_i.Therefrom $\{\dot{R}\}(t_i)$ is derived.Because for uniform strain $\{\dot{R}\}$ is independent of position, the parallel parts of the curves in Fig.13 indicate *macroscopic* strain uniformity.This as one can realize is sweepingly the case during flow instability.

For uniform strain eq(19) gives

$$\dot{\sigma}(t)/M + \dot{\epsilon}_p(t) = \dot{\epsilon}_0 = \text{constant}$$

and therefrom

$$-(1/M)d\dot{\sigma}/dt = d\dot{\epsilon}_p/dt \qquad (23)$$

The analysis of flow behaviour during instability by means of eq(23) is shown in Fig.14.First the strain rate accelerates at σ^*.During the stress drop $d\dot{\epsilon}/dt$ changes the sign and for $\sigma=\sigma_{min}$ the decelaration has a maximum.

Assuming uniform strain,the relationship between the radial $\dot{R}/R_0$ strain rate and the

axial strain ϵ is

$$\dot{\epsilon}_R \equiv -2\dot{R}/R_o = \dot{\epsilon}_o(1+\epsilon)^{-3/2}$$

where the index denotes the initial values.The above equation expresses the kinetic equilibrium between the radial– $\dot{\epsilon}_R$ and axial strain rate $\dot{\epsilon}_o$ resp.For equlibrium and for $\{\dot{R}\} = \dot{R}$ it is

$$-2\{\dot{R}\}(1+\epsilon)^{3/2}/(R_o\dot{\epsilon}_o) = 2(\dot{\epsilon}_R/\dot{\epsilon}_o)(1+\epsilon)^{2/3} \equiv J(\dot{R}) = 1 \qquad (24)$$

In Fig.15b the time dependence of $J(\dot{R})$ is shown for a STC test at 340^{o}C (Fig.15a).By inspection it is obvious that at the early beginning of deformation the strain distribution is not uniform,however it becomes uniform in the course of deformation and proceeds to be uniform also during flow instability.Macroscopic strain loca–lization,i.e.necking,definitely marks failure.Obviously it depends of the defect mobility,i.e. of the growth rate of critical fluctuations whether strain distribution will be macroscopically uniform or will become localized .Accordingly,in contrast to high temperatures,structural instability at low temperatures will be prone to shape instability.

3.Summary and Conclusions

The stability of high temperature plastic flow was examined in terms of the ratio $\lambda=W/W_s$ (expended to stored energy) which is suggested as a measure for the distance from thermodynamical equilibrium.W_s is calculated from an empirical relationship. This for the materials examined is shown to be obeyed in a broad range of temperatures.The critical distance λ_m^* derived from the model is proportional to the critical stress σ^* and is expected to be independent of loading procedure and material.This is confirmed by experiments.Moreover the experimental λ^*–values turned out to be independent of loading path and strain path resp.Hence λ^* reveals the property of a quantity of state.

In view of the present model structural instability is the consequency of the exhaustion of energy storage capability.The latter is a general phenomenon of crystal plasticity and occurs,irrespective of loading conditions and material,at a critical distance λ^* from thermodynamical equilibrium.Structural instability is initiated by growth of critical fluctuations in deformation substructure which in turn give rise to changes in deformation substructure.Macroscopically structural instability reveals as a transient increase in strain rate (flow instability). It depends of the defect mobility,i.e.of the growth rate of critical fluctuations,whether strain distribution remains uniform or will become localized (shape instability). Accordingly,in contrast to high temperatures, structural instability at low temperatures will be prone to necking.Experimental investigations conducted on Cu PCs at $T_h > 0.4$ have shown that strain distribution was macroscopically uniform during flow instability.Structural instability occurs in single crystals as well.The strain to criticality ϵ^* for identical loading conditions turned out to be in Cu SCs substantially larger than for PCs.This obviously demonstrates the fact that,owing to the existence of grain structure,less strain is required to develop a critical deformation structure in PCs.Data analysis reveals a proportionality between the critical size d_s^* of dislocation substructure and the grain size d_g.Although this is not jet understood,there are observations in support of this.

References.

[1] R.L.Amadeo and N.M.Ghoniem,Res Mech.23(1988)137
[2] D.L.Holt,J.Appl.Phys.41(1970)3197
[3] E.C.Aifantis,Mat.Sci.Eng.81(1986)563
[4] D.Walgraef,in F.Tirapequi and D.Villarroel (edts.),Instabilities in Non–Equilibrium Structures, D.Reidel Publishing Company,Hingham,Ma, 1987,p.197
[5] E.C.Aifantis,in L.P.Kubin and G.Martin (edts.),Non Linear Phenomena in Materials Science,Trans.Tech.Publications Ltd,Switzerland,1988,p.397
[6] H.Haken,Advanced Synergetics,Springer,Berlin,1984
[7] M.Bočvek,Z.Metallk.79(1988)132
[8] S.V.Raj and G.M.Pharr,Mat.Sci.Eng.81(1986)217
[9] M.Bočvek,Physica Sripta T29(1989)213
[10] R.O.Williams,Trans.Met.Soc.AIME 224(1962)719
[11] M.B.Bever,D.L.Holt and A.L.Tichener,The Stored Energy of Cold Work, Pergamon Press, Oxford,1973
[12] G.Gottstein,D.Zabardjadi and H.Mecking,Metal Sci.13(1979)223
[13] G.Gottstein and U.F.Kocks,Acta Met.31(1983)175
[14] P.Karduck,G.Gottstein and H.Mecking,Acta Met. 31(1983)1525
[15] V.M.Sample,G.L.Fitzimons and A.J.DeArdo,Acta Met.35(1987)367
[16] M.J.Luton and C.M.Sellars,Acta Met.17(1969)1033
[17] H.P.Stüwe,Z.Metallk.56(1965)633
[18] I.Prigogine,Res Mechanica 21(1987)342
[19] T.Sakai and J.J.Jonas,Acta metall.32(1984)189
[20] M.Bočvek and J.–H.Choi.To be published in:Proceedings of the International Conference on the Mechanics,Physics and Structure of Materials,Thessaloniky, Greece,19–24 August 1990.
[21] P.Karduck,"Untersuchungen zu Keimbildung und Kornwachstum bei dynamischer Rekristallisation von Kupferkristallen".Dissertation,RWTH Aachen,1980
[22] P.Neuhäuser,"Physical Manifestation of Instabilities in Plastic Flow",SMR/154–8, IAEA–Working Party on:Mechanical Properties and Behaviour of Solid–Plastic Instabilities,Trieste,12–20 August 1985
[23] Y.Estrin and L.P.Kubin,Res Mechanica 23(1988)1974
[24] G.Walensi,Rev.Métall.45(1948)10

[25] S.Straub and W.Blum,Scripta metall.materialia 24(1990)1837
[26] T.Sakai and M.Ohashi,Mat.Sci.Technol.6(1990)1251
[27] M.Ueki,S.Horie and T.Nakamuro,Mat.Sci.Technol.3(1987)329
[28] Jae–Ho Choi,Dissertation,Universität Karlsruhe,to appear June 1991
[29] L.Blaz,T.Sakai and J.J.Jonas,Metal Sci.17(1983)609
[30] D.Kuhlmann–Wilsdorf and J.H.van der Merve,Mat.Sci.Eng.55(1982)79

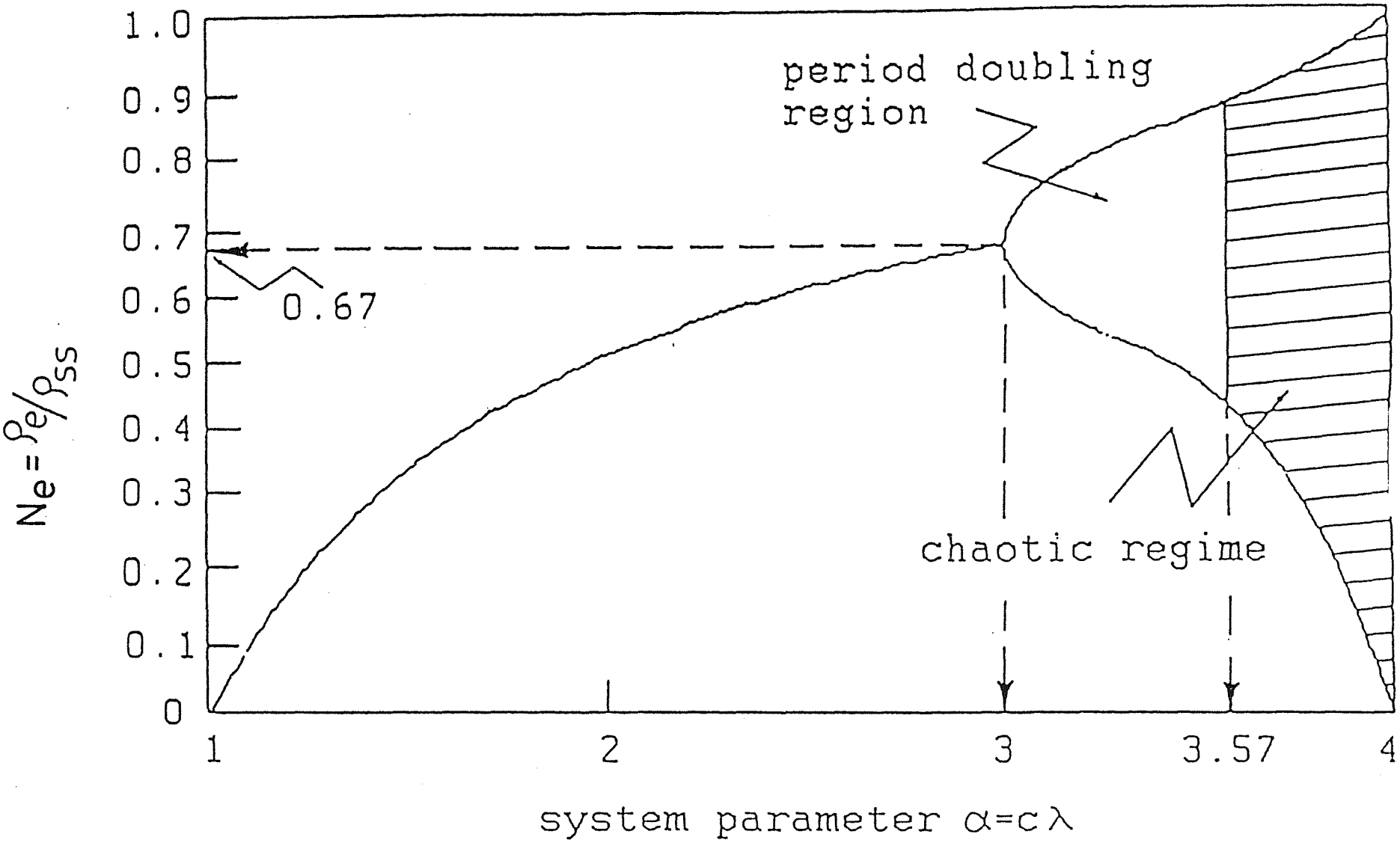

Fig.1 Bifurcation diagram (see text)

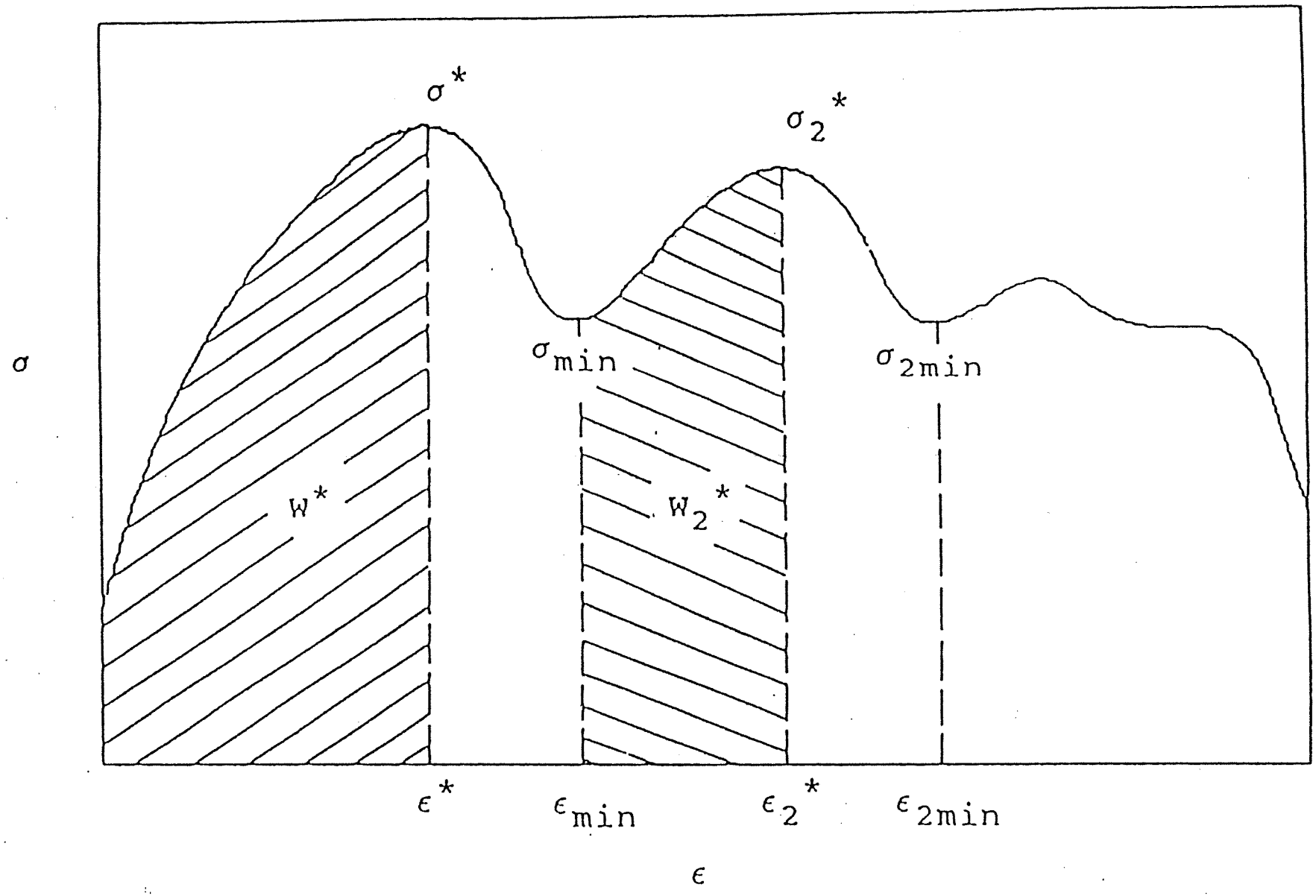

Fig.2 Stress/strain diagram with repeated instability (schematically;actually the critical stress at structural instability is slightly below the stress peak σ^*; see text)

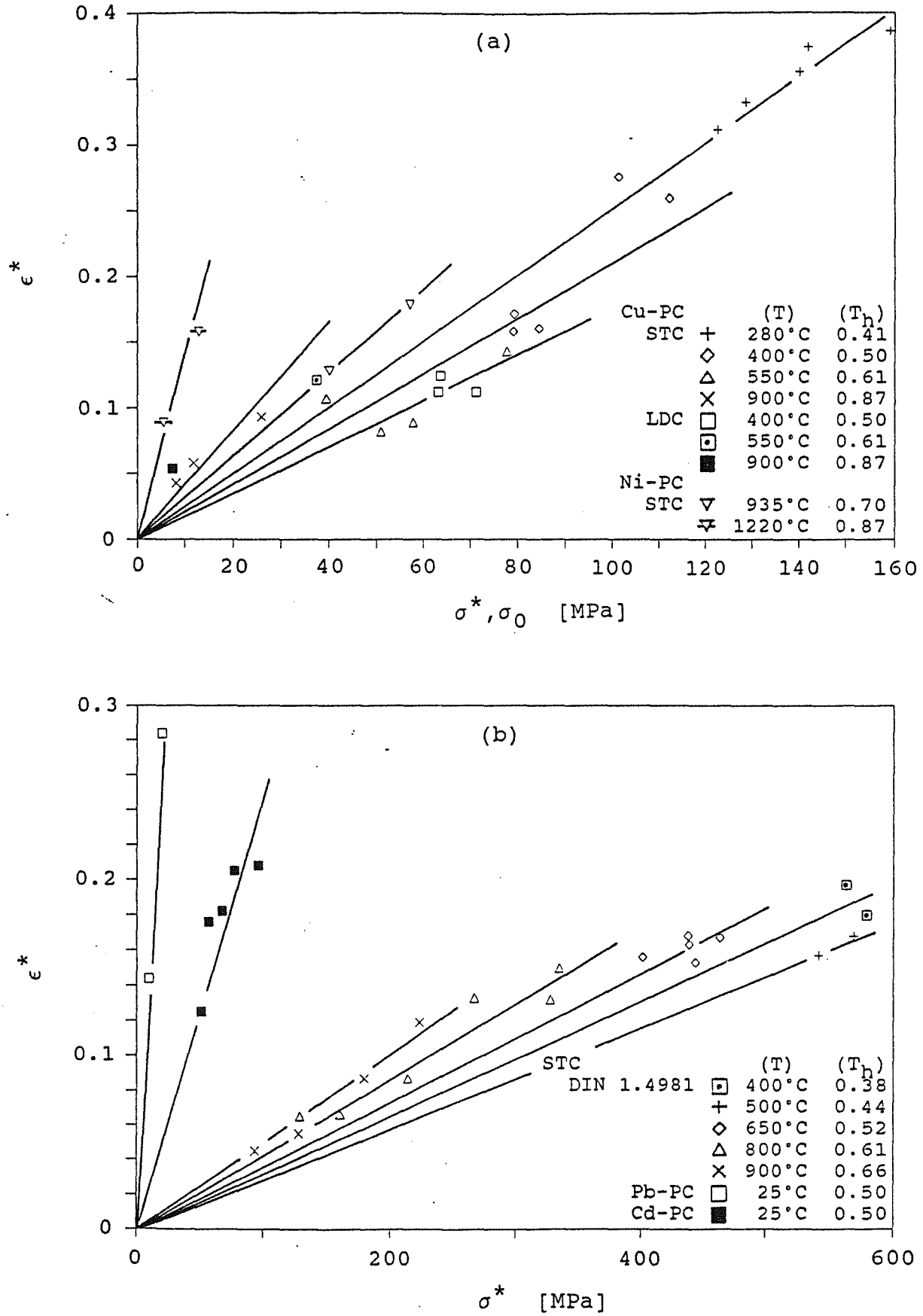

Fig.3 The critical strain ϵ^* vers. σ^*

a) Cu PCs;STC– and LDC tests;Ni PCs,STC tests

b) aust.steel type DIN 1.4981,Cd–,Pb PCs;STC tests.

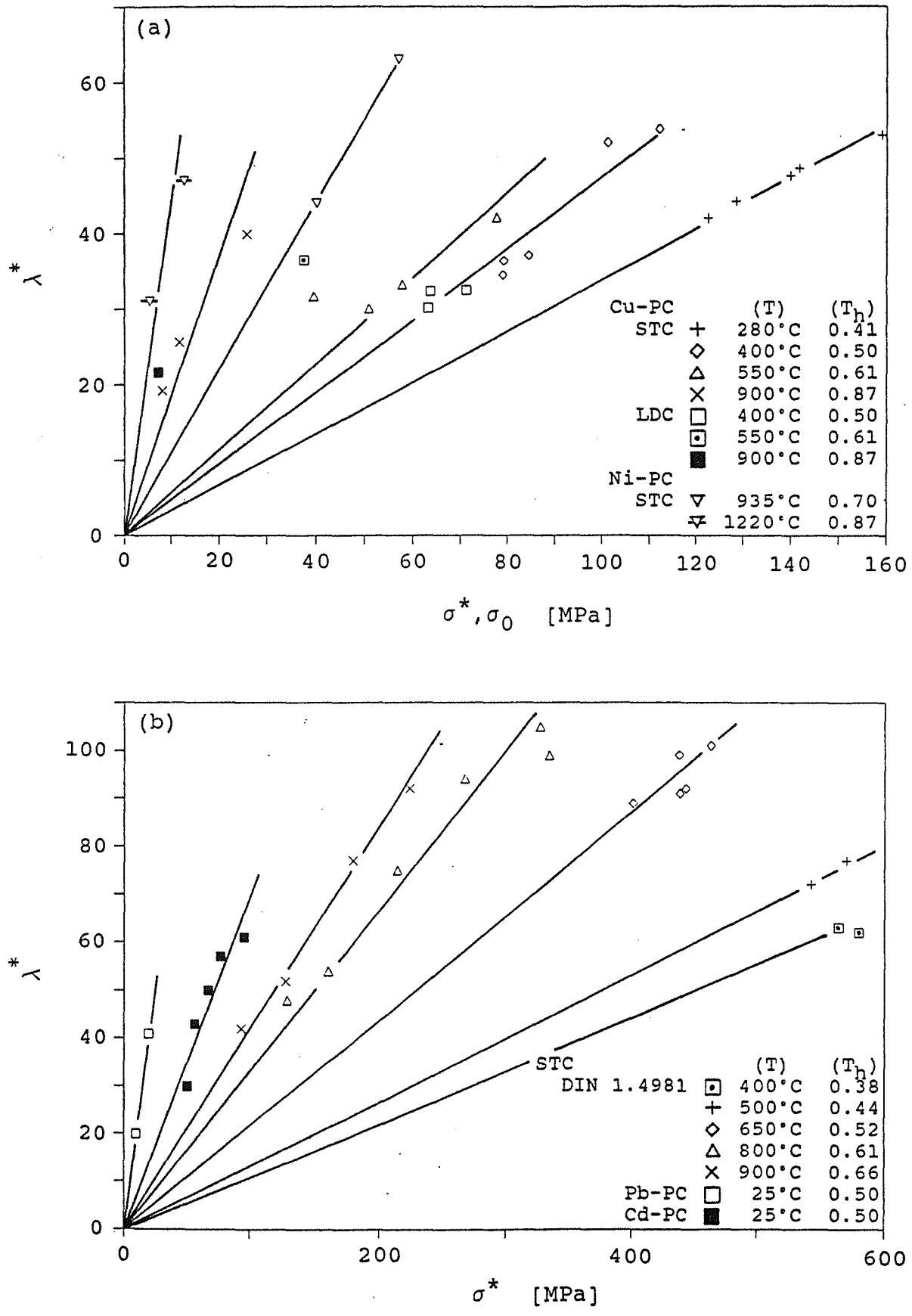

Fig.4 The stress dependence of λ^*

a) Cu PCs;STC– and LDC tests;Ni PCs,STC tests

b) aust.steel type DIN 1.4981,Cd–,Pb PCs;STC tests.

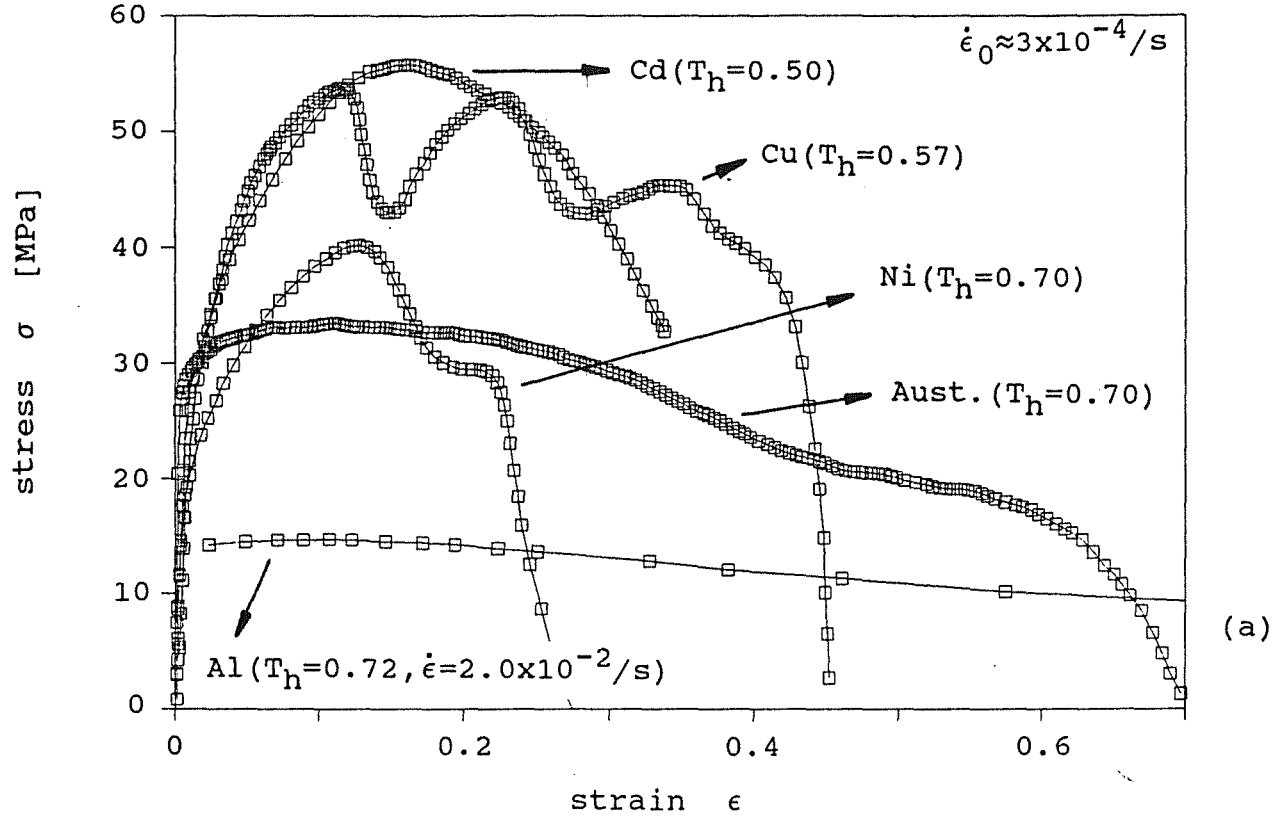

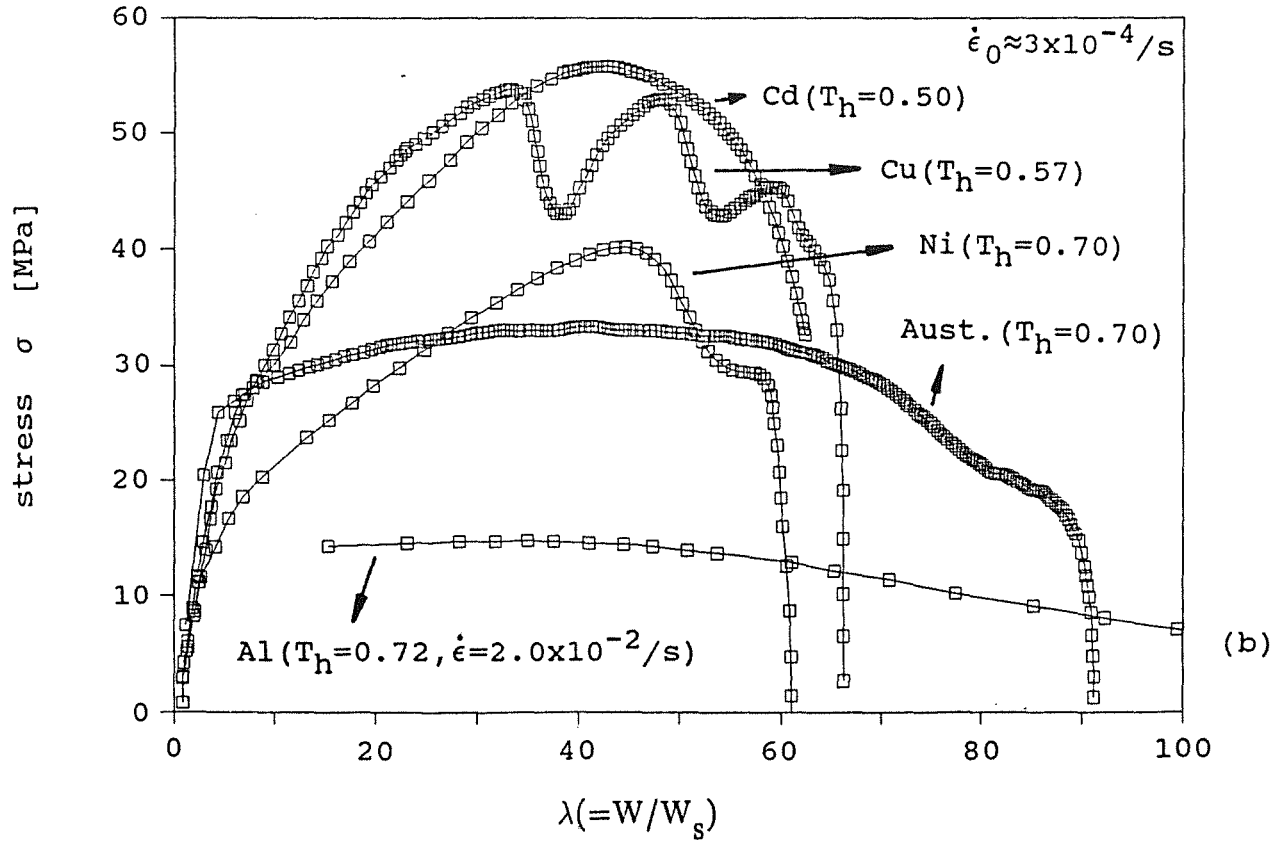

Fig.5a Stress/strain–curves for different materials and temperatures (curve for Al obtained in torsion [17])

Fig.5b Stress vers.λ–curves (derived from Fig.5a,read λ up to λ^*)

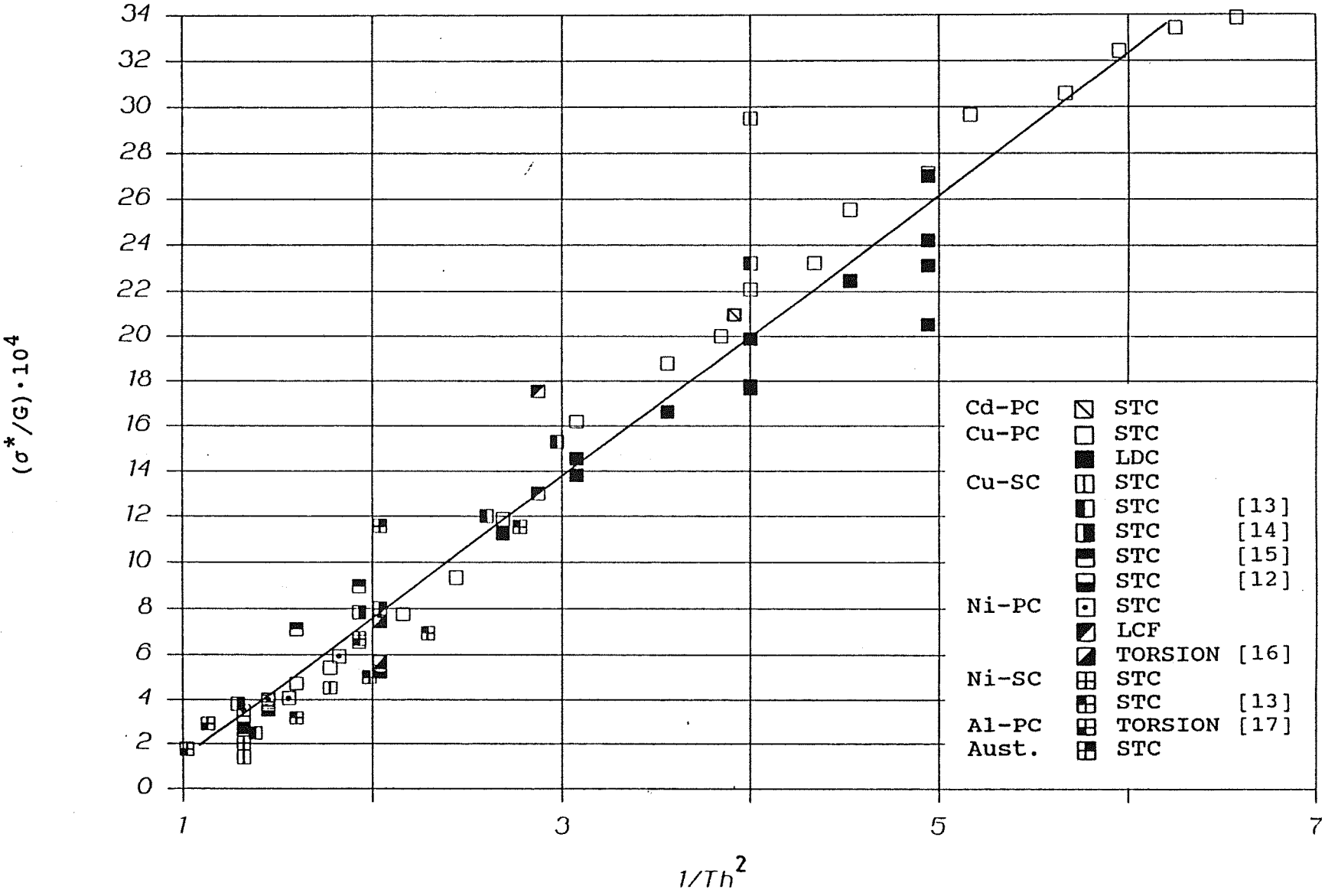

Fig.6 σ^*/G vers.$1/T_h^2$ for different materials and testing procedures.

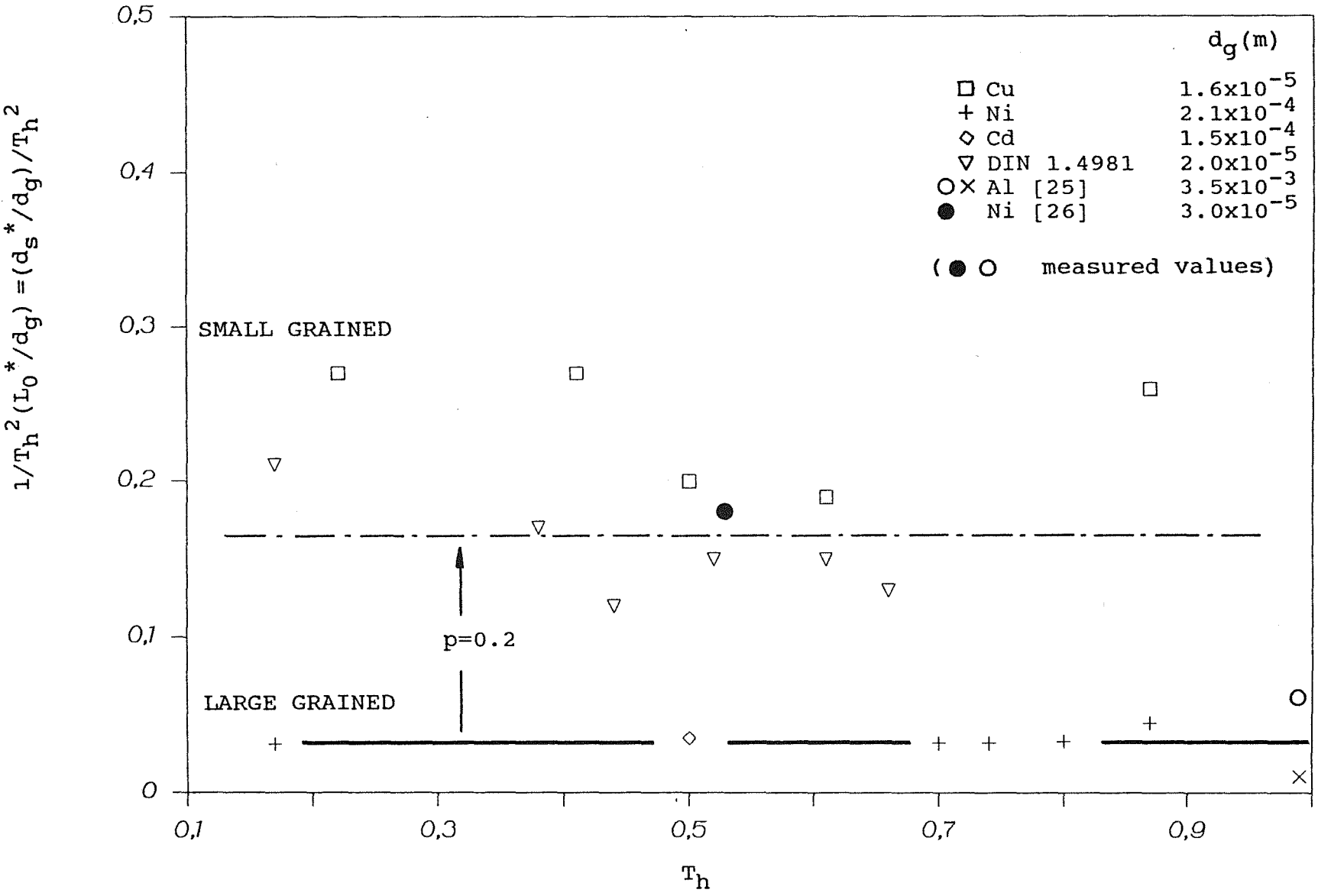

Fig.7 Calculated $(d_s^*/d_g)/T_h^2$–values (p=1) vers.T_h for different materials.For coarse grained materials the mean value calculated with p=0.2 is represented by the dash–dot line.

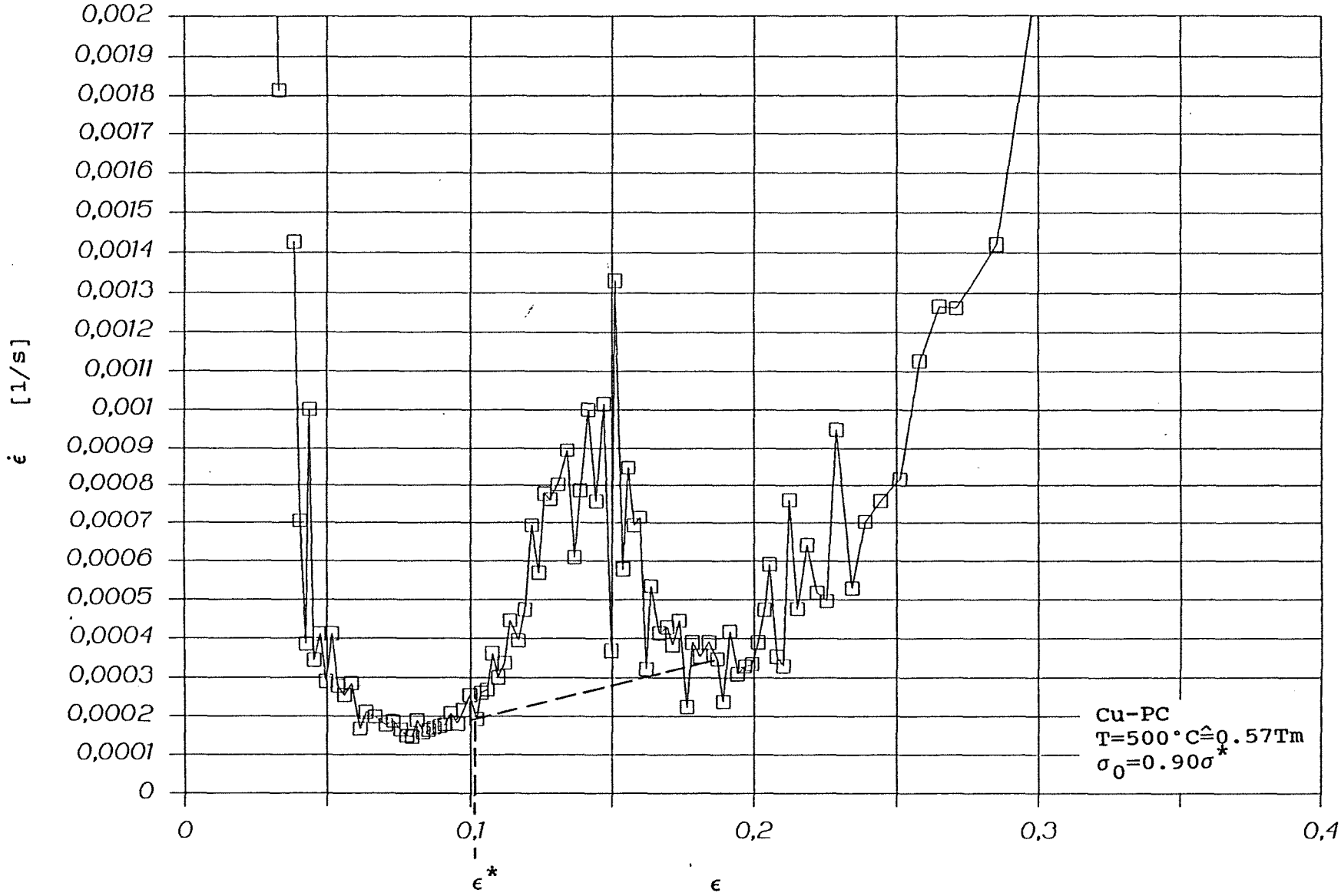

Fig.8 Creep curve of a Cu PC (to be compared with the STC test in Fig.11b at 500^{O}C;see text)

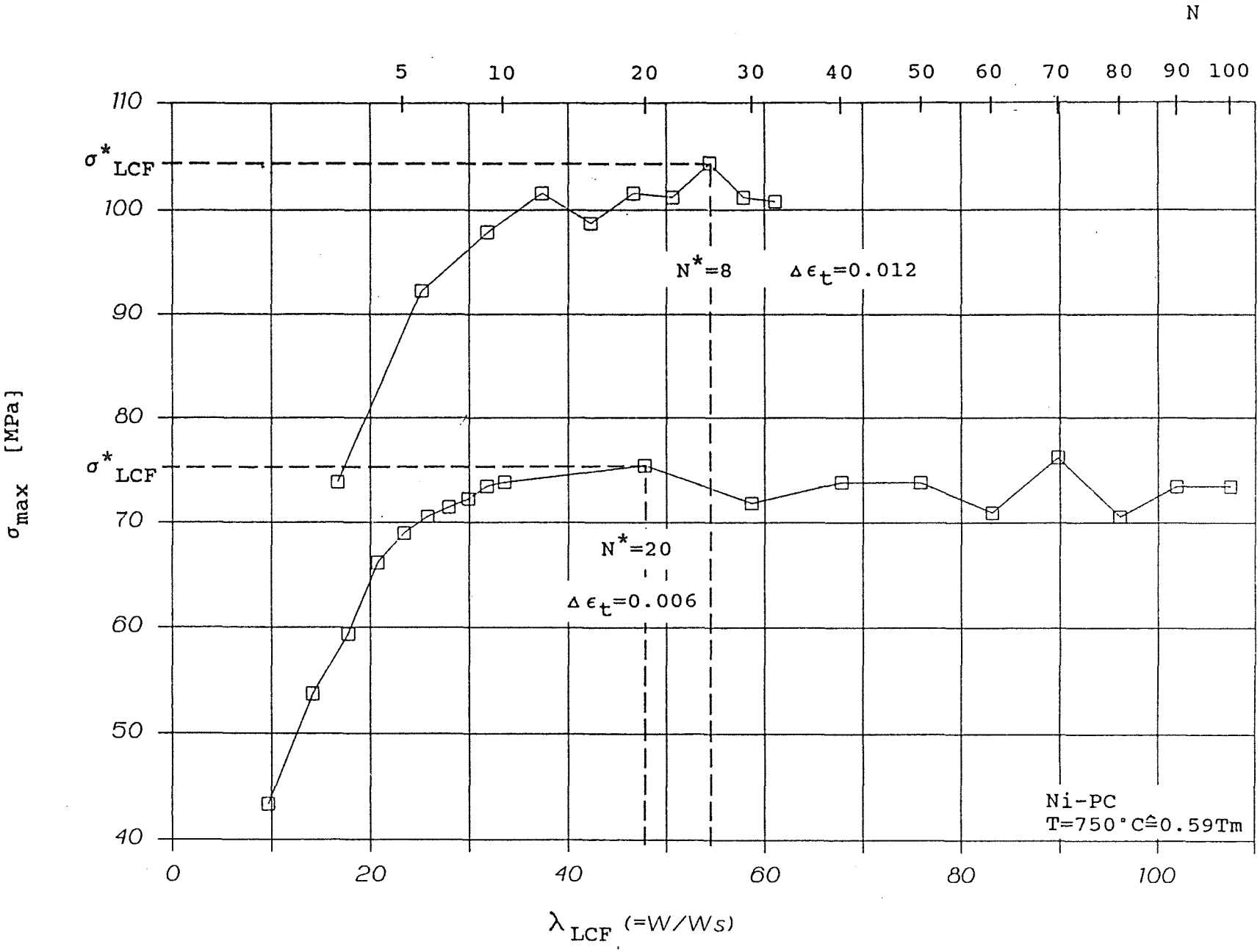

Fig.9 Cyclic hardening curves for Ni–PCs for different total strain amplitude $\Delta\epsilon_t$

(upper scale: number of cycles N ; lower scale: energy ratio λ)

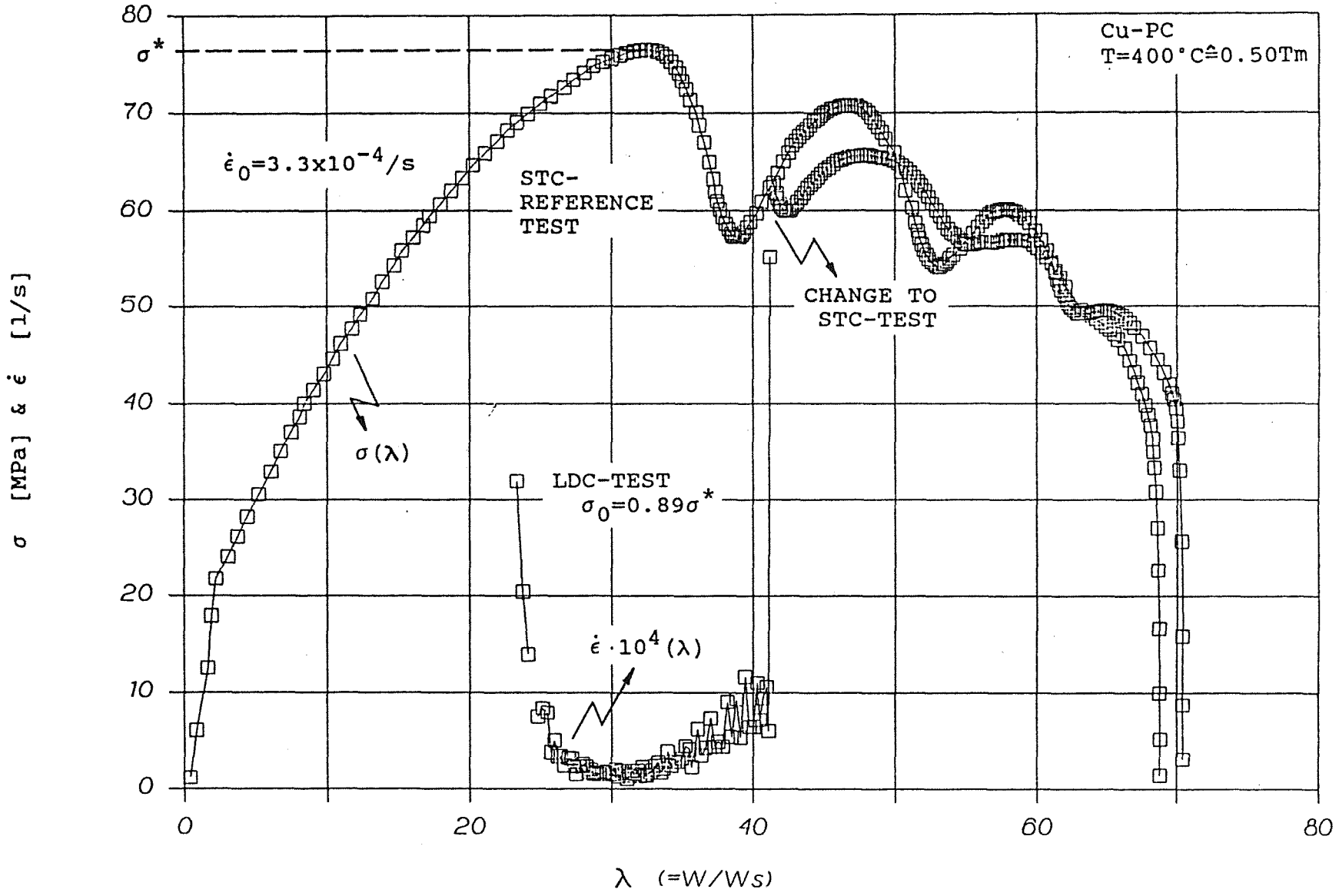

Fig.10 Change–in–loading procedure from LDC to STC test(see text;read λ up to λ^*)

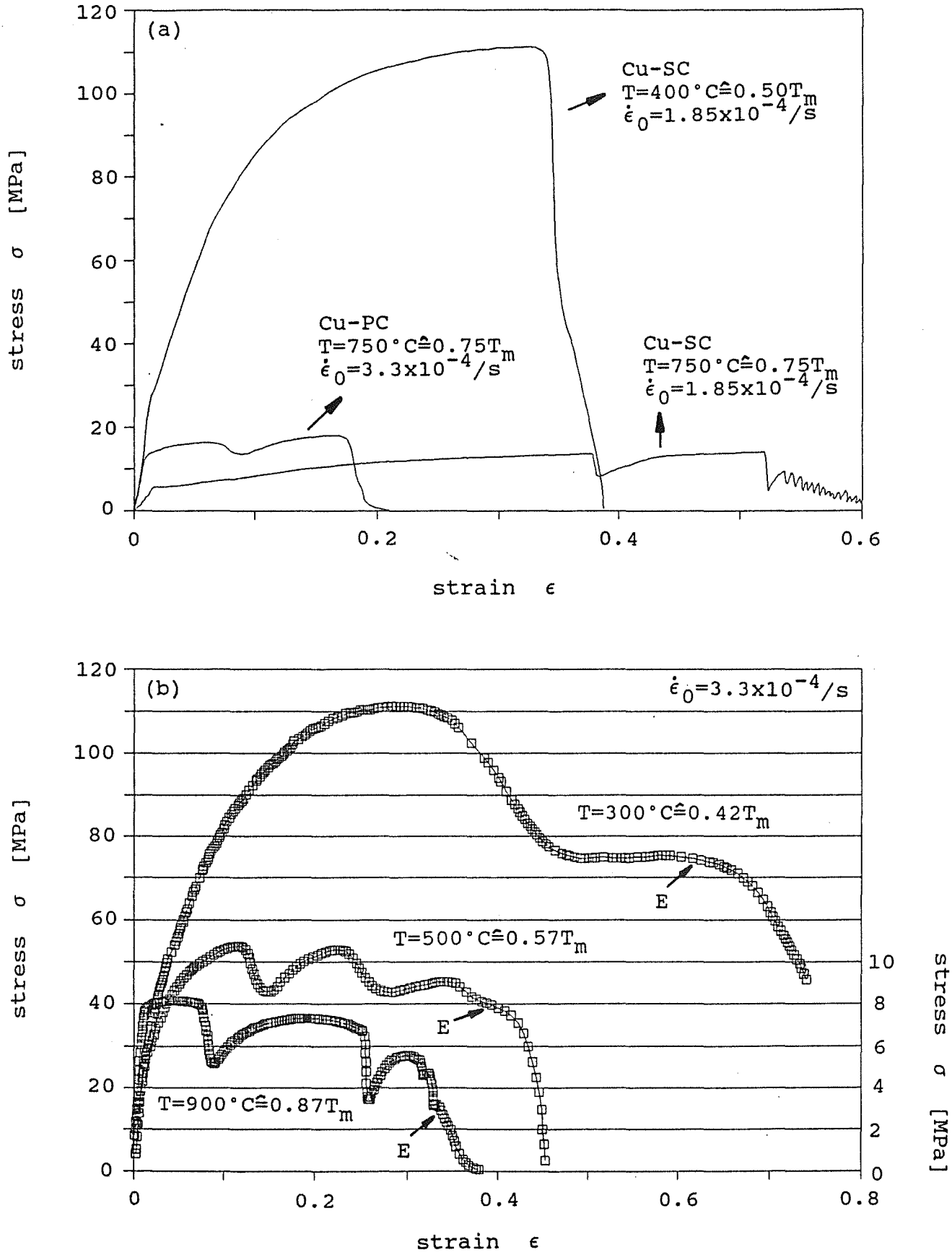

Fig.11 a)Comparison of $\sigma(\epsilon)$–curves for Cu SCs and PC resp.;b) $\sigma(\epsilon)$–curves of Cu PCs;influence of temperature (arrows mark the onset of necking).

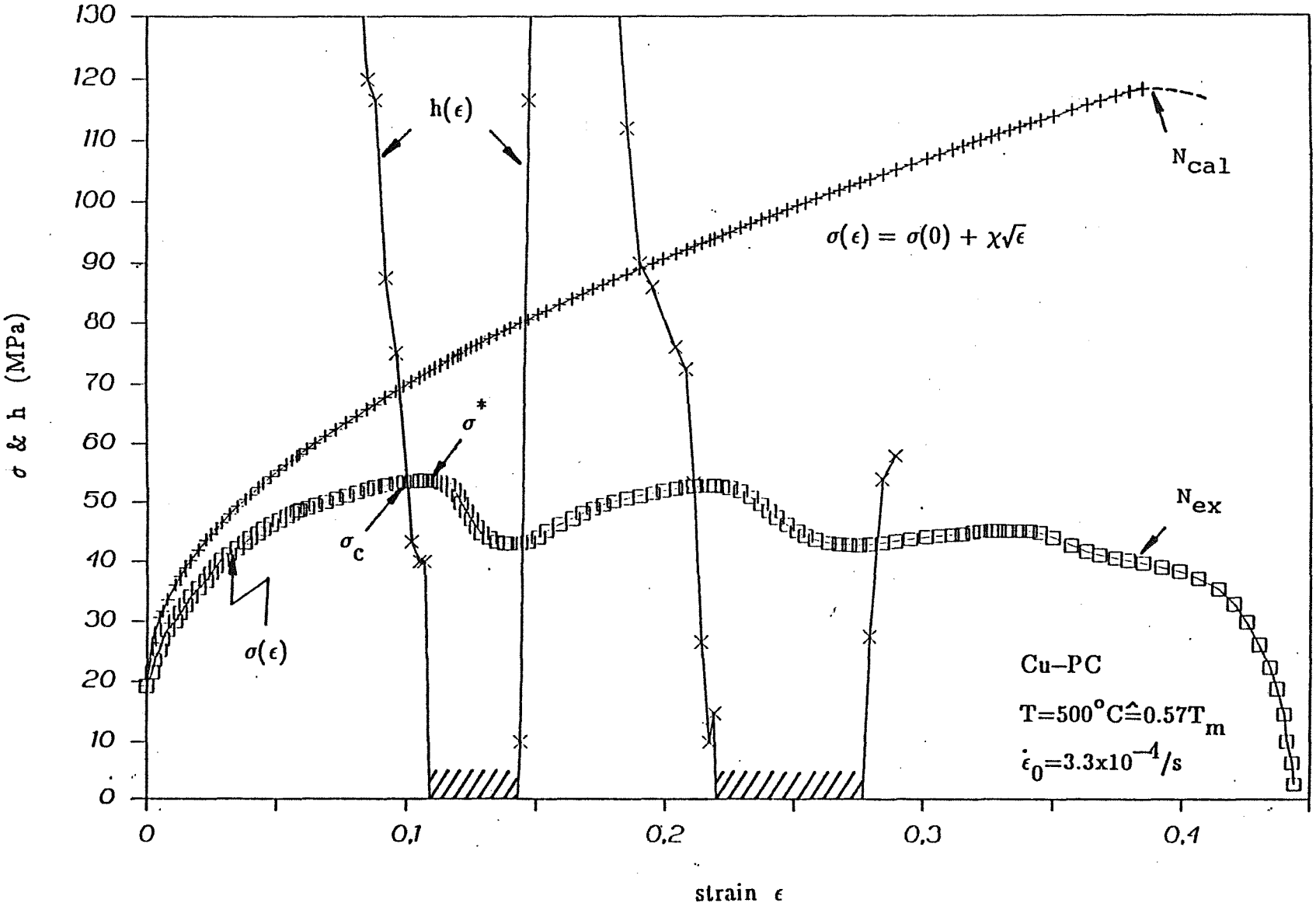

Fig.12 Experimental $\sigma(\epsilon)$– and $h(\epsilon)$–curves for a Cu PC deformed at 500°C;compare with the corresponding calculated $\sigma(\epsilon)$–curve (see text;arrows mark onset of necking).

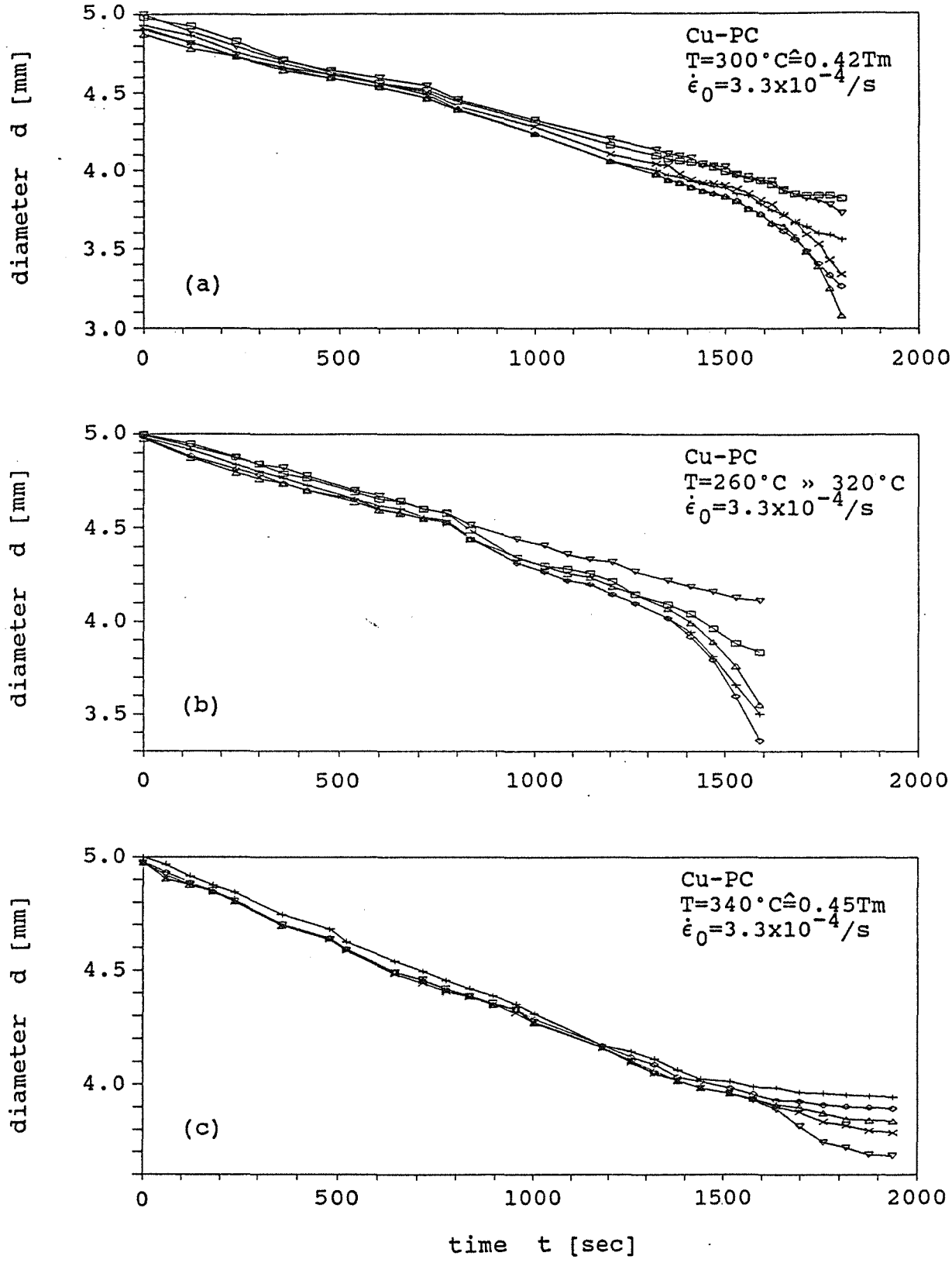

Fig.13 Diameter of the specimen 2R vers.time.(STC tests on Cu PCs at:300,320 and 340^{o}C;see text)

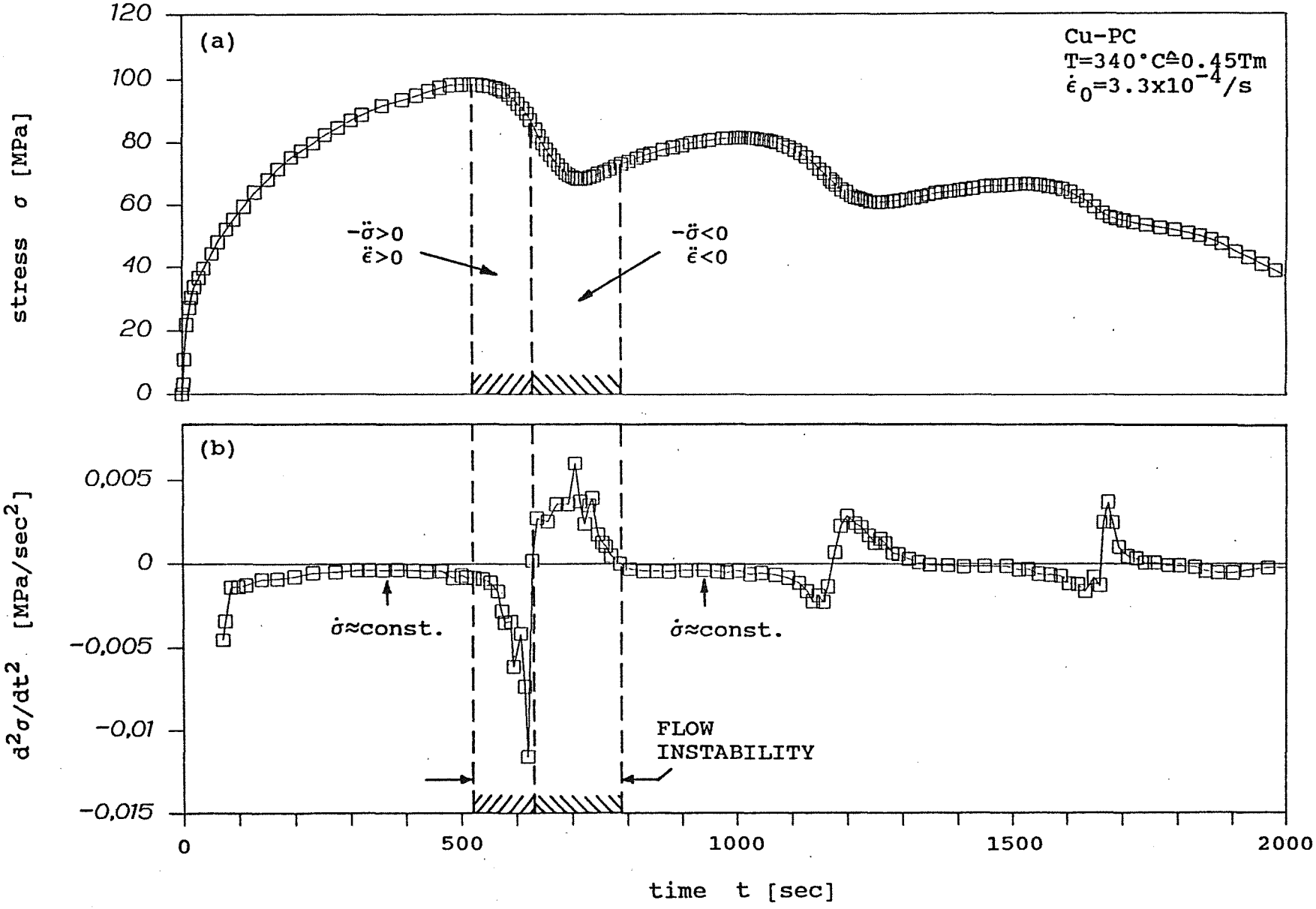

Fig.14 STC test on Cu PC at 340^{o}C. a) σ vers.t; b) $d\dot{\sigma}/dt$ vers.t (see text)

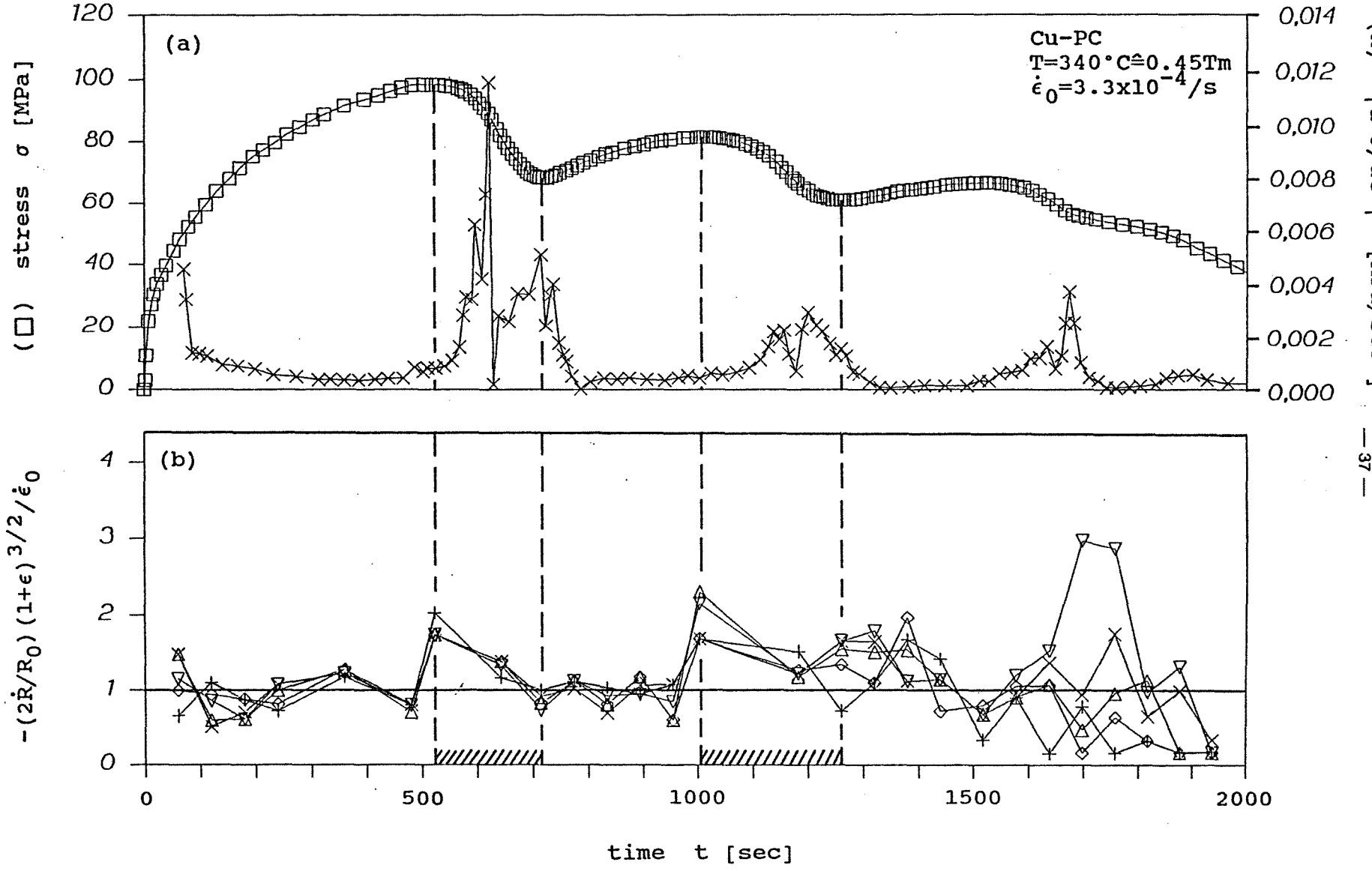

Fig.15 STC test on Cu PC at 340°C. a) σ(t) and $d\dot{\sigma}/dt$ vers.t; b) J($\dot{R}$) vers.t (see text)

Table 1

Data from STC- and LDC-tests for different materials and temperatures

Material	T_h	G[1] in UNITS $[10^{10}Pa]$	$d\lambda^*/d\sigma^*$ $[10^{-7}Pa^{-1}]$	$(d\epsilon^*/d\sigma^*)_{ex}$ $[10^{-9}Pa^{-1}]$	$(d\epsilon^*/d\sigma^*)_{cal}$ $[10^{-9}Pa^{-1}]$	L_0^*/b $[10^3]$	$(L_0^*/d_g)/p$ $(=d_s^*/d_g)$[9] $[10^{-2}]$	$(L_0^*/d_g)/T_h^2$ $=(d_s^*/d_g)/T_h^2$ for p=1	d_g $[\mu m]$
Cu	0.22	4.21	0.81[3]	1.8[4]	1.9	0.81	0.013	0.27	16
	0.41	3.78	3.2	2.6	2.5	2.9	4.6	0.27	16
	0.50	3.58	3.6	2.0	1.4	3.1	5.0	0.20	16
	0.61	3.33	5.7	1.8	1.6	4.5	7.2	0.19	16
	0.87	2.73	19.0	4.0	4.3	12.3	19.7	0.26	16
Ni	0.17	7.9	0.41[3]	1.3[4]	1.5	0.77	0.091	0.032	210
	0.70	5.2	11.0	3.3	3.7	13.6	1.6	0.033	210
	0.74	5.0	13.0[3]	3.9[4]	4.2	15.5	1.8	0.033	210
	0.80	4.7	17.0[3]	5.0[4]	5.2	19.0	2.2	0.034	210
	0.87	4.4	28.0	9.3	10.0	29.3	3.5	0.046	210
	0.59	5.8	5.8[8]	2.2[8]	2.1	8.0			
Cd	0.50	2.78	7.0	2.5	3.0	4.6	0.9	0.036	150
Pb	0.50	0.73	20.1	14.3	17.3	3.5			

(cont.)

Table 1, cont'd

Material	T_h	G[1] in UNITS $[10^{10}Pa]$	$d\lambda^*/d\sigma^*$ $[10^{-7}Pa^{-1}]$	$(d\epsilon^*/d\sigma^*)_{ex}$ $[10^{-9}Pa^{-1}]$	$(d\epsilon^*/d\sigma^*)_{cal}$ $[10^{-9}Pa^{-1}]$	L_0^*/b $[10^3]$	$(L_0^*/d_g)/p$ $(=d_s^*/d_g)$[9] $[10^{-2}]$	$(L_0^*/d_g)/T_h^2$ $=(d_s^*/d_g)/T_h^2$ for p=1	d_g $[\mu m]$
Al[2]	0.57	2.2	8.6[3]	2.8[4]	3.4	4.5			
	0.62	2.2	9.6[3]	2.3[4]	3.1	5.0			
	0.72	2.0	23.7[3]	7.3[4]	10.2	11.3			
	0.75	2.0	19.0	15.0	5.6	9.0			
	0.83	1.9	35.2[3]	10.5[4]	12.8	15.9			
	0.94	1.8	74.8[3]	30.2[4]	35.1	32.1			
	0.99	1.7	107[3]	45.0[4]	58.4	43.3			
Al[5]	0.99	1.7	350[6]	410[7]	620	140	1.1	0.011	3500
DIN 1.4981	0.17	8.2	0.24[3]	0.37[4]	0.46	0.47	0.6	0.21	20
	0.38	7.3	1.1[3]	0.31[4]	0.40	1.9	2.4	0.17	20
	0.44	6.2	1.3[3]	0.29[4]	0.30	1.9	2.4	0.12	20
	0.52	5.7	2.4	0.38	0.53	3.1	4.0	0.15	20
	0.61	5.1	3.5	0.44	0.59	4.3	5.5	0.15	20
	0.66	4.7	4.4	0.54	0.68	4.6	5.9	0.13	20
DIN 1.4909	0.70	4.2	12.4[3]	3.3[4]	4.3	12.4	2.7	0.055	120

(cont.)

Table 1, cont'd

1) All constants from H.J.FROST and M.F.ASHBY,
Deformation mechanism maps, Pergamon Press, Oxford 1982

2) H.P.STÜWE, Z.Metall. 56(1965)633

3) λ^*/σ^*

4) ϵ^*/σ^*

5) From LDC test S.STRAUB and W.BLUM,
Scripta Metall. Materialia 24(1990)1837

6) λ^*/σ_0 (σ_0 nominal creep stress)

7) ϵ^*/σ_0

8) From LCF test, mean values from Table 2

9) For p=1

Table 2

Data from LCF tests on Ni polycrystals

(T=1023K$\hat{=}$0.59Tm)

ϵ^*/σ^* [$10^{-9}Pa^{-1}$]	$\Delta\epsilon_t$	σ^*_{LCF} [MPa]	N^*	ϵ^*_{LCF}	W_C [J/gatom]	W^*_{LCF} [J/gatom]	λ^*_{LCF}	λ^*/σ^* [$10^{-7}Pa^{-1}$]
3.2	0.006	75.5	20	0.24	3.3	66.0	50	6.6
2.1	0.012	90.0	8	0.19	9.2	74.0	52	5.8
1.7	0.012	105	8	0.19	9.2	74.0	52	4.9
1.7	0.016	96.0	5	0.16	14.2	71.0	52	5.4
2.4	0.020	99.0	6	0.24	20.4	122.4	62	6.3

Table 3

Change in loading procedure experiments on Cu polycrystals

		W_0	W_1	λ^*_{CLC}
REFERENCE	LDC (σ_0=71.2MPa)			λ^*_R=33
	STC			λ^*_R=33
Cu 116	LDC (σ_0=71.4MPa)	37		
	STC		26	34
Cu 123	LDC (σ_0=71.4MPa)	42		
	STC		20	34
Cu 124	STC	13		
	LDC (σ_0=76.4MPa)		42	32
Cu 146	STC	13		
	LDC (σ_0=71.3MPa)		40	31

$T=400°C(\hat{=}0.5T_m)$, $\dot{\epsilon}_{STC}=3.3\times10^{-4}/s$

Table 4

Data from STC tests on Cu single crystals

T [°C]	T_h	$\dot{\epsilon}_0$ [1/s]	σ^* [MPa]	ϵ^*	W^* [J/gatom]	λ^*	sp/mp
400	0.50	1.85×10^{-4}	105.6	0.33	200.6	60	sp
550	0.61	1.85×10^{-4}	37.5	0.13	22.6	30	sp
750	0.75	1.85×10^{-4}	13.7	0.38	27.8	52	mp
750	0.75	1.85×10^{-4}	12.8	0.29	20.7	45	mp
750	0.75	1.85×10^{-3}	24.4	0.18	19.8	44	sp
750	0.75	1.85×10^{-2}	30.1	0.15	21.7	46	sp
900	0.87	1.85×10^{-4}	7.0	0.39	15.9	51	mp

(sp...single peak, mp...multiple peak flow behaviour)